

AMERICAN UNIVERSITY OF BEIRUT

SIZING OF A FUEL CELL STACK AND BATTERY
SYSTEM FOR A FUEL CELL HYBRID VEHICLE USING
DYNAMIC PROGRAMMING AND PARETO ANALYSIS

by
HANI ABDEL KARIM SADEK

A thesis
submitted in partial fulfillment of the requirements
for the degree of Master of Science
to the Department of Mechanical Engineering
of the Faculty of Engineering and Architecture
at the American University of Beirut

Beirut, Lebanon
April 2019

AMERICAN UNIVERSITY OF BEIRUT

SIZING OF A FUEL CELL STACK AND BATTERY SYSTEM
FOR A FUEL CELL HYBRID VEHICLE USING DYNAMIC
PROGRAMMING AND PARETO ANALYSIS

by
HANI ABDEL KARIM SADEK

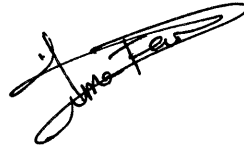
Approved by:

Riad Chedid, Professor
Electrical and Computer Engineering



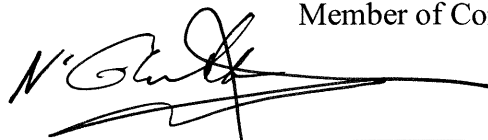
Advisor

Dima Fares, Lecturer
ProGreen Online Program



Co-Advisor

Nesreene Ghaddar, Professor
Mechanical Engineering



Member of Committee

Sami Karaki, Professor
Electrical and Computer Engineering



Member of Committee

Date of thesis defense: April 15, 2019

AMERICAN UNIVERSITY OF BEIRUT

THESIS, DISSERTATION, PROJECT RELEASE FORM

Student Name:

SADER

HANI

ABED EL KARIM

Last

First

Middle

Master's Thesis Master's Project Doctoral Dissertation

I authorize the American University of Beirut to: (a) reproduce hard or electronic copies of my thesis, dissertation, or project; (b) include such copies in the archives and digital repositories of the University; and (c) make freely available such copies to third parties for research or educational purposes.

I authorize the American University of Beirut, to: (a) reproduce hard or electronic copies of it; (b) include such copies in the archives and digital repositories of the University; and (c) make freely available such copies to third parties for research or educational purposes after : **One** ---- year from the date of submission of my thesis, dissertation, or project.
Two ---- years from the date of submission of my thesis, dissertation, or project.
Three ---- years from the date of submission of my thesis, dissertation, or project.



April 30, 2019

Signature

Date

ACKNOWLEDGMENTS

First and foremost, I thank my advisor Professor Riad Chedid for his continued and highly valuable guidance and constructive criticism. Special thanks also go to co-advisor professor Dima Fares for the appreciated time and constant support.

Sincere appreciations are extended to all the committee members with great gratitude to the Director of Masri Institute; Professor Nesreen Ghaddar and Chairman of the Electrical and Computer Engineering Department; Professor Sami Karaki. Their contributions undeniably shone great light to this Thesis, and I admire their vision, value their input, and highly esteem their contributions.

Finally, I thank my family and friends for their patience while I researched, debated, analyzed, tested and wrote to then finally present this Thesis.

AN ABSTRACT OF THE THESIS OF

Hani Sadek for Master of Science
Major: Energy Studies

Title: Sizing of a fuel cell stack and battery system for a fuel cell hybrid vehicle using dynamic programming and pareto analysis

In this study we analyzed fuel cell hybrid electric vehicle models to identify the optimal size combination of fuel cells and batterie. This was in order to attain the lowest hydrogen consumption per trip. To achieve this goal, we used a tunnel dynamic programming technique to perform the optimal energy management strategy for each size combination. Battery selection is done based on different parameters in order to attain the most appropriate type. Two driving modes – charge sustaining and charge depleting - are obtained by adding a weight to battery cost in the optimization function. PARETO analysis is considered to find the best solution that secures the most appropriate battery and fuel cell sizes as well as the least operational cost for three specific driving cycles. Drivability constraints -gradeability, maximum speed and maximum acceleration - were taken into consideration during the sizing process. Different sizing combinations were obtained for the two driving modes over the three different driving cycles.

CONTENTS

ACKNOWLEDGMENTS.....	V
ABSTRACT	VI
LIST OF ILLUSTRATIONS	X
LIST OF TABLES	XII
LIST OF ALGORITHMS	XIII
Chapter	
1. INTRODUCTION.....	1
1.1 Literature Review	2
1.2 Thesis Contribution	9
1.3 Abbreviations.....	10
2. MODELING THE FCHV	11
2.1 Overview of FCHV Difference from EV	11
2.2 FCHV Model	12
2.3 Vehicle Dynamic System	13
2.4 Fuel Cell System Model	16
2.5 Battery Selection and System Model.....	24
2.6 Electric Motor.....	30

2.7	Transmission.....	31
2.8	Auxiliaries	31
3.	DRIVING CYCLES.....	33
4.	PROBLEM DEFINITION	37
5.	ENERGY MANAGEMENT SYSTEM.....	38
5.1	Tunnel Dynamic Programming for Optimum power Allocation	39
5.2	Operation Modes	49
6.	POWER SOURCES SIZING OPTIMIZATION.....	51
6.1	Drivability Constraints	51
6.1.1	Maximum Speed.....	51
6.1.2	Gradeability	52
6.1.3	Acceleration.....	52
6.1.4	Combined Constraints	54
6.2	Pareto Front	55
7.	RESULTS.....	57
7.1	Highway.....	58
7.1.1	CD Mode	59
7.1.2	CS Mode.....	61
7.2	FUDS	62

7.2.1 CD Mode	64
7.2.2 CS Mode.....	65
7.3 NEDC	67
7.3.1 CD Mode	68
7.3.2 CS Mode.....	70
7.4 Summary.....	71
8. CONCLUSION	73
Appendix	
1: ABBREVIATIONS	74
REFERENCES.....	75

ILLUSTRATIONS

Figure	Page
2.1 Topology of Fuel Cell Electric Vehicle.....	13
2.2 Forces Acting on the Vehicle	15
2.3 FCHEV Power Propagation	16
2.4 H5000 Fuel Cell	17
2.5 Fuel Cell Block.....	18
2.6. Fuel Cell System Components (Marx et al., 2017)	18
2.7. H5000 Efficiency Curve (Marx et al., 2017).....	20
2.8 H5000 Voltage-Current Curve (Store, 2013)	21
2.9 H5000 Hydrogen Consumption Curve (Store, 2013).....	21
2.10 H5000 Power-Current Curve (Store, 2013).....	21
2.11 Fuel Cell Equivalent Circuit Model	22
2.12 Battery Equivalent Circuit Model	26
2.13 MC_AC124_EV1 Motor Efficiency Map	30
2.14 FCHEV Main Auxiliaries.....	32
3.1 Highway Driving Cycle Speed and Demand Power Profiles.....	33
3.2 FUDS Driving Cycle Speed and Demand Power Profiles	34
3.3 NEDC Driving Cycle Speed and Demand Power Profiles.....	35
5.1 FCHEV Energy Management System.....	38
5.2 FCHV Electric Power Flow.....	39
5.3 Tunnel Dynamic Programming Sketch	41
5.4 Example of Tunnel Dynamic Programming - Forward Path.....	42
5.5 Example of Tunnel Dynamic Programming - Backward Path.....	43

5.6 Tunnel Dynamic Programming Forward Algorithm (Fares et al., 2015).....	46
5.7 FCHV Operating Modes - Charge Sustaining & Charge Depleting	49
6.1 Vehicle Speed Profile for Maximum Acceleration Constraint.....	53
6.2 Power Demand for the Maximum Acceleration Constraint.....	54
6.3 Combined Drivability Constraint Specifying the Feasible Region	55
7.1 Trip Cost Contour Plot for Highway Driving Cycle	58
7.2 Pareto Front for Highway Driving Cycle	58
7.3 Power Allocation and State of Charge for Charge Depleting Mode - Highway	59
7.4 Power Allocation and State of Charge for Charge Sustaining Mode - Highway	61
7.5 Trip Cost Contour Plot for FUDS Driving Cycle.....	62
7.6 Pareto Front for FUDS Driving Cycle.....	63
7.7 Power Allocation and State of Charge for Charge Depleting Mode - FUDS	64
7.8 Power Allocation and State of Charge for Charge Sustaining Mode - FUDS	65
7.9 Trip Cost Contour Plot for NEDC Driving Cycle	67
7.10 Pareto Front for NEDC Driving Cycle.....	67
7.11 Power Allocation and State of Charge for Charge Depleting Mode - NEDC.....	68
7.12 Power Allocation and State of Charge for Charge Sustaining Mode - NEDC.....	70

TABLES

Table	Page
2.1 Vehicle Variables and Parameters.....	14
2.2 H5000 Fuel Cell Characteristics.....	24
2.3 Lithium Base Battery Properties (Battery Univeristy, 2016, July 21)	27
2.4 Lithium Nickel Manganese Cobalt Oxide Cell Properties (Battery Univeristy, 2016, July 21).....	27
2.5 Lithium Nickel Cobalt Aluminum Oxide Cell Properties (Battery Univeristy, 2018, May 31)	28
2.6 Lithium Titanate Cell Properties (Battery Univeristy, 2018, May 31).....	28
2.7 Lithium Titanate Battery Properties Chart (Battery Univeristy, 2018, May 31)	29
3.1 Driving Cycles Characteristics Summaries	35
7.1 Simulation Results for Highway in Charge Depleting Mode.....	60
7.2 Simulation Results for Highway in Charge Sustaining Mode.....	62
7.3 Simulation Results for FUDS in Charge Depleting Mode	65
7.4 Simulation Results for FUDS in Charge Sustaining Mode	66
7.5 Simulation Results for NEDC in Charge Depleting Mode	69
7.6 Simulation Results for NEDC in Charge Sustaining Mode	71
7.7 Results Summary.....	71

ALGORITHMS

Algorithm	Page
5.1 Tunnel Dynamic Programming (Fares et al., 2015).....	42
6.1 Sizing Simulation Algorithm.....	56

CHAPTER 1

INTRODUCTION

Both research and development can drive innovation, growth, efficiency, and productivity, as well as improved human living standards. Undoubtedly, health is a significant factor in living standards, and the environment is a crucial element contributing to healthy living. Our environment today is plagued by pollution that is primarily caused by carbon dioxide emissions which are released by the internal combustion engines relying on fossil fuels.

Vehicle manufacturers are competing to produce more environmentally friendly vehicles, following extensive work done by research and development units, electric vehicles have been brought to the market as such solutions. The limitations to currently marketed electric powered vehicles can be mitigated by the introduction of FCHV relying on both batteries and fuel cells that use hydrogen from renewable energy sources.

Hydrogen is the most abundant chemical element on earth and is characterized by its extremely high energy capacity compared to batteries. The fuel cell in electric vehicles can eliminate pollution as it produces zero emissions, especially if hydrogen was produced by using renewable energy. Hydrogen has a high specific energy when compressed (40 kWh/kg) which is more than 200 times the specific energy of a high energy capacity lithium ion battery. Hydrogen is lightweight by nature and can power a FCHV for long ranges without increasing the volume or weight of the energy storage system in the vehicle. This advantage can be a solution for the aviation industry in the future as batteries will occupy large spaces in the cargo if they were the only source of power. Larger weights and volumes require stronger vehicle frame and higher

propulsion torque. These requirements limit the range the pure electric vehicles can travel. Moreover, FCHV can be refueled in minutes while the pure electric vehicles take hours to be recharged. Range and refueling times are two major advantages that make the FCHV more interesting to the automotive industry and the car manufacturers.

The challenge that remains is finding the right balance of fuel cells and batteries for electricity generation as well as the right number of fuel cell stacks, the right storage systems, the right sizes, and, ultimately, the right mix and appropriate usage of fuel cells and batteries. Extensive research still needs to be done to reach the most cost-effective, economically feasible and efficient solution for mass production of FCHV.

The cost-effective sourcing of hydrogen, as well as the ability to store hydrogen over longer times, are important in making this a more user-friendly (less fueling stops required for longer driving distances) and commercially viable solution in replacing fossil fuels. Multi-stack fuel cells (MFC) are considered to be an answer to the storage lifetime dilemma, while they also entail additional costs and present more management challenges and user inconveniences.

We are still at the early stage of mass manufacturing of these types of vehicles, but it will be quickly advanced given that consumers and regulators are pushing for more environmentally friendly and sustainable solutions for the currently highly global polluting transportation sector. The FCHV will prove to be a highly wanted product, not just because they are the latest fad, but for the sake of a better quality of life for all humankind.

1.1 Literature Review

Previous studies were conducted on HEV and they addressed different design parameters. Many researchers focused on exploring the advantages and challenges of

hybridization. Roda et al. modified an electric vehicle by adding to it a fuel cell. In their paper, they presented the advantages of using a hybrid system compared with pure electric. Their model was tested for more than one thousand hours of the fuel cell and proved its reliability.(Roda, Carroquino, Valiño, Lozano, & Barreras, 2018). Aschilean et al. presented a study on the addition of a fuel cell to a pure electric vehicle. To experiment with their research, they replaced an internal combustion engine of a jeep wrangler with a fuel cell/battery hybrid system. They also discussed the economic advantages such a system would gain when the price of the fuel cell decreases in the future.(Aschilean et al., 2018)

Fathabadi presented a combination of a 90-kW fuel cell and a 19.2 kWh lithium-ion battery. He showed the advantages of using such a combination based on the increased efficiency of the system and the extended cruising range of the vehicle. He also discussed how advantageous a FCHV is compared with internal combustion engine vehicles. Later, he added to the previous combination a 600 F supercapacitor. He showed that his proposed model attained higher driving powers and met higher drivability requirements than other configurations.(Fathabadi, 2018, 2019)

In addition, researchers also worked on showing the importance of an optimized EMS in the HEV. Sulaiman et al. discussed the importance of the EMS and explained its role in energy and cost saving as well as the prolongation of battery and fuel cell lives. They also gave several recommendations about the development and implementation of the optimized EMS.(Sulaiman et al., 2018). Lü et al. wrote a general paper presenting a SWOT analysis for the use of plug-in FCHV. Moreover, they explained the EMS used by many researchers and presented their advantages and challenges. Finally, they gave their opinion about the need to improve the system

response to the changes in the dynamics of the system, the service lifetime, the economic optimization, and the overall efficiency.(Lü, Qu, Wang, Qin, & Liu, 2018)

One of the major advantages of hybridization presented by researchers was the importance of regenerative braking. Li et al. proposed a regenerative braking energy recovery strategy in a fuel cell/supercapacitor hybrid system. Their approach is based on Pontryagin's Minimum Principle, and their research results showed how energy absorption could be optimized and reused to meet the drastic changes in energy demand. (Li et al., 2019). Ahmadi et al. studied the effect of different driving cycles and the degradation of the fuel cell on the economy of the vehicle. They explained the importance of capturing the energy regenerated from braking, especially in the driving patterns where there are a lot of starts/stops from relatively high speeds.(P. Ahmadi et al., 2019)

Several researchers worked on the operation of the EMS and they tried to solve the optimization problem using different techniques and strategies. Tazelaar et al. solved the optimization problem analytically. Their work provided a comprehensive understanding of the optimization problem. They compared the analytical results with experiments and simulation, and the margin of error was negligible (less than 1%)(Tazelaar, Veenhuizen, & Grimminck, 2012). Taherzadeh et al. proposed a new strategy for plug-in HEV with internal combustion engines being the primary source of energy. They set the operation mode of the ICE at its maximum efficiency depending on the driving cycle, and made the battery respond to the variation of the demand. Their strategy illustrated that they could achieve a significant decrease in fuel consumption.(Taherzadeh, Dabbaghjamesh, Gitizadeh, & Rahideh, 2018). Fonseca et al. applied the same strategy but on a fuel cell instead of ICE. They fixed the operation rate of the fuel cell at its maximum efficiency and made the battery respond to the

dynamic variation of demand.(da Fonseca et al., 2012). Odeim et al. conducted other research through which he compared an offline optimization technique based on DP with real-time optimization. The real-time optimization parameters were taken from the optimal results of the offline optimization. The final results show that real-time optimization consumed slightly more fuel, but its control was better for power sources degradation. Odeim et al. also introduced an approach to the optimization and the design of the EMS of a hybrid power system having three sources of power (fuel cell/battery/supercapacitor). The parameters of their strategy were optimized by a Genetic Algorithm and a Pareto front analysis. They validated their results using a test bench composed of the three sources mentioned earlier. In addition, Odeim et al. compared two online and real-time optimization methods. The first used a PI controller whose operation is based on Pontryagin's Minimum Principle with three control parameters and the second used a Fuzzy controller with ten control parameters. Their results showed that the PI controller performed better than the Fuzzy controller although it had a smaller number of control parameters. (Odeim, Roes, & Heinzl, 2015, 2016; Odeim, Roes, Wülbeck, & Heinzl, 2014). Dinnawi et al. used a Linear Programming technique for energy management to reduce consumption and operational cost. They compared their simulation results with those of a vehicle simulation software over HW and FUDS driving cycles. (Dinnawi, Fares, Chedid, Karaki, & Jabr, 2014). Marx et al. conducted a study on the effect of hybridization on the fuel economy and power sources degradation rates. They used a Rule-Based energy management technique and relied more on the battery. They concluded that a better fuel economy and lower fuel cell degradation rates could be achieved with higher hybridization. (Marx, Hissel, Gustin, Boulon, & Agbossou, 2017). Fares et al. developed an efficient EMS using a DP technique. To test their system, they used a model based on Simulink

architecture of an electric vehicle. They achieved a hydrogen consumption saving of 15% on HW and 50% on FUDS compared with the Rule-Based technique. (Fares et al., 2014; Fares, Chedid, Panik, Karaki, & Jabr, 2015). Fletcher et al. worked on reducing operating costs using Stochastic DP technique for the EMS. They achieved a decrease of 12.3% in the cost of operation and an increase of 14% in the lifetime of the fuel cell, but the fuel consumption increased by 3.5%.(Fletcher, Thring, & Watkinson, 2016). Wang et al. showed how DP solves the numerical issues associated with the optimization problem. They also showed how DP helped to reduce the fuel consumption of a plug-in HEV by 20% compared with traditional control methods. The results obtained were used to calibrate other online optimization strategies. (Wang, He, Sun, & Zhang, 2015). Karaki et al. used the Forward DP technique to optimize the EMS for a FCHV for CD and CS modes over two standard driving cycles, UDDS and HWFET. The study was performed for different vehicle weights, fuel cell sizes, and battery energy and power capacities. Their primary objectives were to reduce hydrogen utilization. They compared their simulation results with those of a Quadratic technique.(Karaki, Jabr, Chedid, & Panik, 2015). Xiao et al. compared three strategies for the EMS -DP, Convex Optimization, and CS/CD algorithm- for a parallel plug-in HEV. Their results showed that by using DP, they achieved lower fuel consumption. However, the lower computational time was that of the Convex Optimization algorithm. (Xiao et al., 2018). Ahmadi et al. designed an EMS based on the Fuzzy logic control algorithm. They tested their strategies on an urban/highway combined cycle and compared their results with others from an advanced vehicle simulator (ADVISOR), and the results they achieved were acceptable. (S. Ahmadi, Bathaee, & Hosseinpour, 2018). Geng et al. introduced a new on-off control strategy and compared it with a Fuzzy algorithm. They conducted the study theoretically, and they ran simulations.

Their results showed that the Fuzzy algorithm performed better than the new strategy.(Geng, Jin, & Zhang, 2019). Denis et al. proposed a Genetic Algorithm that reduced the time of calculation in the EMS. The computation time obtained was smaller than that of DP, but there was an error of 1.9% in the SOC and an increase of 2.8% in the consumption of fuel. (Denis, Dubois, Trovão, & Desrochers, 2018). Bizon et al. explained the main issues and challenges for real-time optimization techniques for a fuel cell/battery hybrid power system. They proposed a new RTO based on Global Extremum Seeking algorithm. Their study was performed on static and dynamic power loads, and they achieved a high rate of savings compared with static feedforward real-time strategy. (Bizon & Thounthong, 2018). Amamou et al. studied a control strategy for electric vehicles to provide the energy required efficiently. They considered both single step and multi-step optimal feedback control and achieved from 8% to 20% savings compared to the results of thermostatic control.(Amamou, Ziadia, Kelouwani, Agbossou, & Dube, 2018)

Other researchers extended their optimizations researchers beyond the optimization of the EMS by finding the best power sources combination for optimal energy saving. Sarma et al. presented a different methodology for the optimization of power sources sizing. They proposed different energy management strategies and incorporated them into a Particle Swarm optimization algorithm to achieve the optimum size. They concluded that the best size combination highly depends on the EMS strategy and the driving cycle characteristics.(Sarma & Ganguly, 2018). Rurgladdapan et al. used DP for optimal power allocation during the driving cycle and analyzed the effect of changing the battery size on the ten years operational cost and came up with the optimal combinations for different driving mileages per year.(Rurgladdapan, Uthaichana, & Kaewkham-ai, 2013; Sarma & Ganguly, 2018).

Song et al. proposed a two-dimensional Pontryagin's Minimum Principle optimization for the power sources sizing and EMS in a plug-in FCHV. Their study showed that fuel consumption dramatically decreased with the increase in battery size and the supercapacitor size up to a particular value.(Song et al., 2018). Tazelaar et al. presented a method for sizing the power sources in a fuel cell hybrid truck. For the EMS, he used different strategies: DP and Equivalent Consumption Minimization strategy. Their Results concluded that the power of the fuel cell should be three times the average of the driving cycle power demand and the battery should supply the difference between the peak power demand and the power of the chosen fuel cell. (Tazelaar, Shen, Veenhuizen, Hofman, & Van den Bosch, 2012). Vinot et al. proposed a sizing method for the battery in a FCHV using the Pareto front. For the EMS, he used Discrete DP algorithm. Their results showed that there is a trade-off between hydrogen consumption and the number of battery modules and it is different for each driving cycle. (Vinot, Reinbold, & Trigui, 2016). Zheng et al. researched the sizing optimization of the power sources in a FCHV and they adopted a Pontryagin's Minimum Principle algorithm for the EMS. Their results showed that the optimal size combination for the lowest cost is different from that of the lowest hydrogen consumption. (Zheng et al., 2014). Karaki et al. used Ordinal Optimization method to find the best combination of FCHV components with the target of achieving the cheapest cruising cost over the year. They adopted DP as a strategy for the EMS. They conducted the study on a combination of two driving cycles: UDDS (45%) and HWFET (55%). They represented the best results for different vehicle specifications based on predefined drivability requirements. (Karaki, Dinnawi, Jabr, Chedid, & Panik, 2015). Hu et al. used a Convex Optimization algorithm to determine the best power split strategy and the optimal power sources sizes of a hybrid bus. They stated that this strategy was efficient and overcame the

burden of heavy computation. They concluded that the power sources sizes are related to the average and standard deviation of the power demand; The battery size is related to the distribution of regenerated energy, and the vehicle economy is highly dependent on the driving cycle smoothness. (Hu, Murgovski, Johannesson, & Egardt, 2015)

Moreover, some researchers explained how choosing the type of the battery and the correct gear ratio can affect the operational cost of the system. Koniak et al. conducted a comprehensive study on the types of batteries that can be used for the automotive application. They considered different factors in their comparison of the different kinds and explained how selecting the correct type of cells result in lower cost of operation.(Koniak & Czerepicki, 2017). Cano et al. provided an exhaustive assessment of different types of batteries and fuel cells that can be used for the automotive application. Their evaluation was based on the range, the cost, and utilization rates. They concluded that lithium-ion batteries grant the best combination of properties for the application mentioned earlier, but a mix of both batteries and fuel cell is still the best solution for reliable and clean transportation.(Cano et al., 2018). Karaođlan et al. investigated the variation in fuel consumption based on the value of gear ratios used in the vehicle. The study showed that emissions and fuel consumption can be reduced not only by hybridization but also by choosing the correct gear ratio.(Karaođlan, Kuralay, & Colpan, 2019)

1.2 Thesis Contribution

Previous studies focused on the optimization of the EMS using different techniques. Others added the sizing optimization of either one or both of the power sources - the fuel cell and the battery - in the HEV using different strategies.

In this thesis, Pareto Analysis is used to find the optimal combination of power sources in a FCHEV leading to the lowest cost of driving. Pareto will help find the best compromise between two conflicting objectives, the battery size and the operation cost, for each fuel cell size.

In addition, TDP is adopted as the optimization strategy to find the optimal power split between battery and the fuel cell for three different driving cycles (Highway, FUDS & NEDC). TDP is an improved version of DP that overcomes the dimensionality problem. This technique was presented and proved efficient by Fares et al. (Fares et al., 2015)

Moreover, this work includes the presentation of the change in the SOC of the battery during the driving cycle for two modes: CD and CS. These modes are attained by the addition of a battery weighting factor to the cost function.

Minimum drivability constraints are considered and taken into account during the optimization. The selection of the suitable type of the battery is also discussed and illustrated.

1.3 Abbreviations

The list of abbreviations used in this thesis is presented in Appendix A

CHAPTER 2

MODELING THE FCHV

2.1 Overview of FCHV Difference from EV

Electric and FCHV have many similarities. They are both driven by electric motors, and they both produce no emissions that harm the environment. However, they are different in many aspects such as the power source, EMS, the cruising range, the charging time and the energy capacity of power sources.

Electric vehicles are powered only by batteries and require simple energy management. The battery is the primary source of power that drives the motor and captures the energy from regenerative braking. The electric vehicles cruising range varies from 90 to 500 km depending on the vehicle model and the size of the battery used. The range of an EV decreases as the battery state of health declines. To charge an electric vehicle, it takes from 30 min to 5 hours depending on the charging mode and the cruising range of the car. The maximum battery energy capacity doesn't exceed 300 Wh/kg, and this is the main reason that limits its cruising range.

Fuel cell electric vehicles are powered mainly by the fuel cells, and the battery acts as a secondary source of energy. The fuel cell generates electric energy in-situ and supplies the motor with the required power. But a fuel cell cannot solely drive the motor as it cannot respond to the dynamic changes in the load, and it can't capture the energy from the regenerative braking, which requires the necessity of a battery. The fuel cell sources of energy are compressed hydrogen, which is stored on board, and oxygen from the air. The FCHEV needs a complicated EMS to manage the power allocation between the fuel cell and the battery. The FCHV's range - 400 to 600 km – is longer than the EV's and can be refueled in 3 to 5 min depending on the tank capacity

and the cruising range. The energy capacity of compressed hydrogen can reach 40,000 Wh/kg giving the FCHEV a significant advantage over the EV in terms of cruising range.

2.2 FCHV Model

The FCHV model consists of 7 main subsystems, as shown in figure 2.1. The first two subsystems are the fuel cell and the energy storage, which are the primary and the secondary sources that supply the power to drive the vehicle. The fuel cell is a one-directional source of DC power while the battery is a bi-directional DC source of power. The battery supplies the power stored and captures the net excess power from the system. When the vehicle is in the motoring mode, the energy that flows from the fuel cell system passes through a DC/DC converter, for the voltage to get stabilized, before moving to another stage in the process. After getting stabilized, the power generated by the fuel cell system, along with the power supplied by the energy storage system, flow through the DC/AC inverter. The DC/AC inverter has the function to transform the DC power to the AC power required to power the induction motor of the vehicle. The electric motor converts electrical energy to rotational mechanical energy. The transmission system in the FCHV changes the rotational speed and the torque according to a specific single gear ratio to meet the requirement of the driving cycle. Finally, the wheels serve as the final subsystem in the FCHV. They are supplied with mechanical power from the transmission system, and their primary function is to move the vehicle.

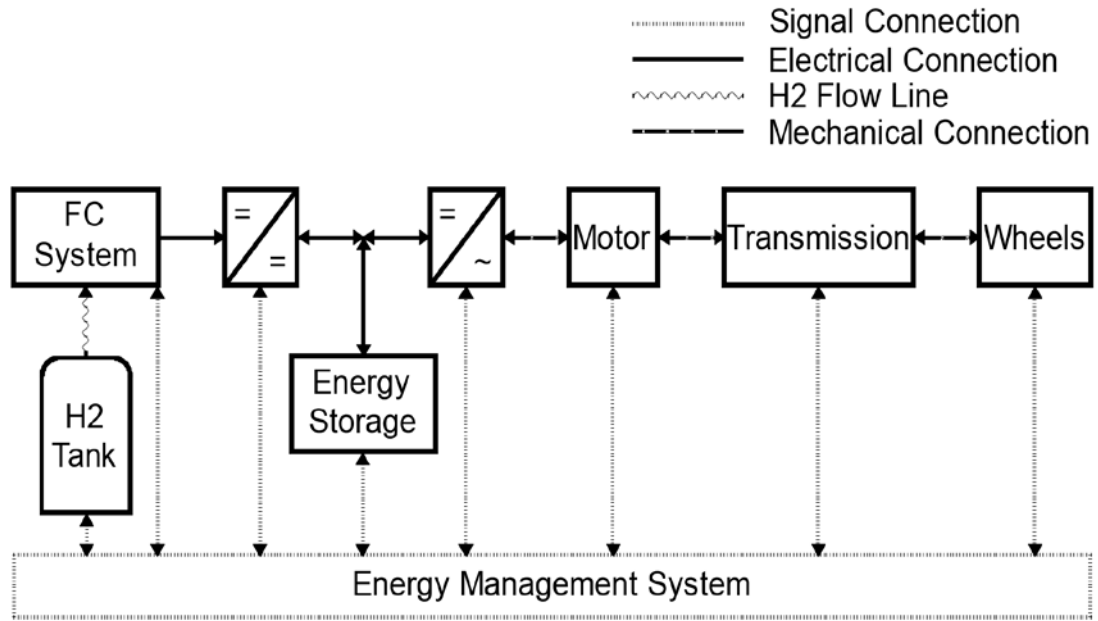


Figure 2.1 Topology of Fuel Cell Electric Vehicle

The same system operates in the reverse direction when the vehicle is in the braking mode. The kinetic energy of the vehicle will be transformed into electric energy by the motor that will act as an alternator, and then the power gets rectified and stored in the energy storage system.

During the driving process, all the subsystems' parameters are monitored and controlled by an EMS installed in the vehicle.

2.3 Vehicle Dynamic System

The parameters considered in the study are all presented in table 2.1. The mass of the electric motor, load, hydrogen tank and the wheel radius are all based on the study conducted by Karaki et al. (Karaki, Dinnawi, et al., 2015)

Variables and Parameters		
Vehicle Mass	1500	kg
Electric Motor Mass	186	kg
Load Mass	320	kg
Frontal Area	2.2	m ²
Aerodynamics Drag Coefficient	0.3	

Rolling Resistance Coefficient	0.009	Ω
Wheel Radius	0.31	m
Hydrogen Tank Capacity	5	kg
Hydrogen Tank Mass	44.5	Kg
Gravitational Acceleration	9.81	m/s ²
Air Density	1.21	kg/m ³

Table 2.1 Vehicle Variables and Parameters

There are four forces that act on the vehicles when travelling on a certain drive terrain: the aerodynamic drag force, the gravitational force, the rolling resistance force and the acceleration force. All the forces are graphically represented in figure 2.2.

The aerodynamic drag force is caused by the compression of air on the frontal surface of the vehicle. it is related to the air density ρ , the frontal surface area of the vehicle A_f , the drag coefficient C_w , and the traveling velocity v . It is mathematically represented by the equation below:

$$F_w = \frac{1}{2} \rho A_f C_w v^2 \quad (2.1)$$

The gravitational force is caused by the load of the vehicle and it only affects the movement of the vehicle when travelling on an inclined road. It is a function of the vehicle mass m , the gravity constant g , and the inclination angle α . It is mathematically represented by the equation below:

$$F_g = mg \sin(\alpha) \quad (2.2)$$

The rolling resistance force is caused by the friction of the wheel on the road surface. It varies with the mass of the vehicle m , the gravity constant g , the rolling resistance coefficient C_r and the inclination angle α . It is mathematically represented by the equation below:

$$F_r = mg C_r \cos(\alpha) \quad (2.3)$$

The acceleration force is required for the acceleration of the vehicle and it is directly related to the mass of the vehicle m and its needed acceleration a . It is mathematically represented by the equation below:

$$F_a = ma \quad (2.4)$$

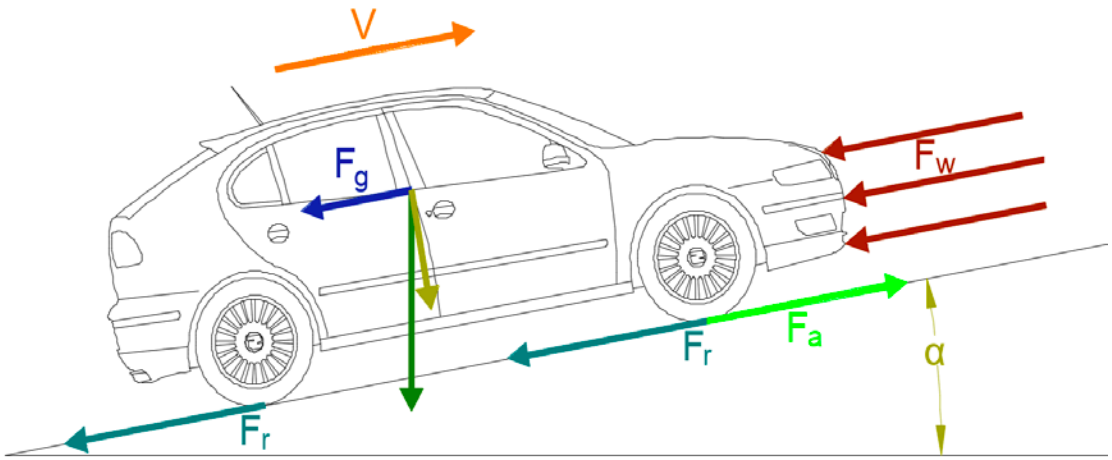


Figure 2.2 Forces Acting on the Vehicle

The total sum of forces (F_T) is the force required to calculate the power demand from the electric motor.

From the total sum of forces calculated in the previous section, the power demanded by the vehicle at the wheels P_{wheels} is calculated as shown in the equation below:

$$P_{wheels} = vF_T \quad (2.5)$$

The power losses in the electric motor and the transmission system should be taken into consideration when calculating the electric power load. It is represented in the equation below:

$$P_L = P_{wheels} + P_{Mloss} + P_{Tloss} \quad (2.6)$$

Power losses in the electric motor and the transmission system will be calculated based on the efficiencies of each one of them. We should also account for the power required by the FCHV auxiliaries P_{aux} . The total electric power demand from the electric power sources is mathematically represented in the equation below:

$$P_{dem} = P_L + P_{aux} \tag{2.7}$$

The power demand propagation through the FCHV is graphically represented in figure 2.3

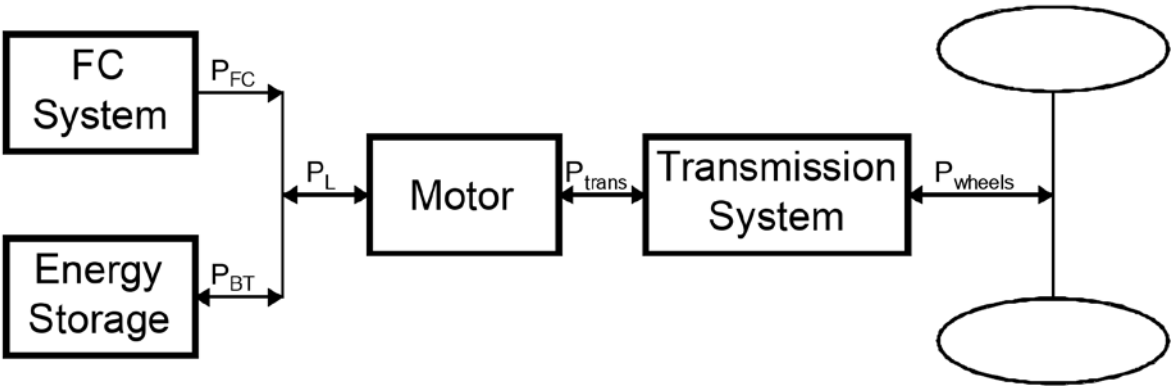


Figure 2.3 FCHEV Power Propagation

2.4 Fuel Cell System Model

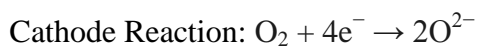
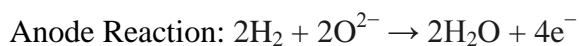
As mentioned earlier, fuel cells will be the primary source of energy in the FCHV system. The Fuel Cells will be composed of modular multi-stack, in addition to their required auxiliaries which are: the power converters, cooling systems, and reactant supply ancillaries.



Figure 2.4 H5000 Fuel Cell

The PEMFC is made from an electrolyte membrane sandwiched between a positive electrode which is the cathode, and a negative electrode which is the anode as shown in the figure 2.5.

The chemical reactions that take place inside the fuel cell are shown in the equations below:



A single fuel cell cannot alone supply a significant amount of power, which is why they are stacked together to reach the required amount of voltage and power.

The PEMFC requires the availability of three additional subsystems: The air supply compressor, the water management system, and the thermal management system.

The air supply compressor ensures supplying enough oxygen to the fuel cell depending on the power demand. The water management system humidifies the air entering to ensure a good conductivity at the membrane level. The thermal management system is

used to maintain the best operating temperature for the electrochemical reaction inside the fuel cell.

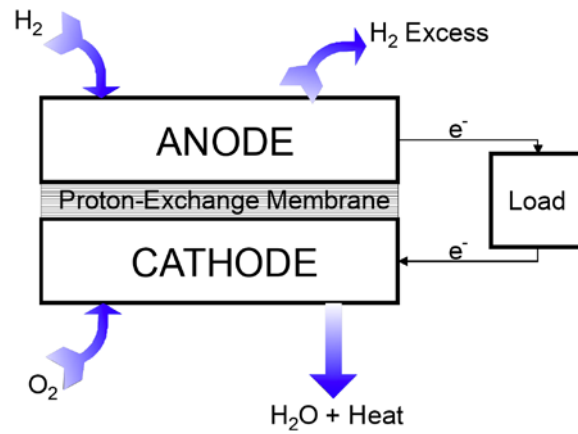


Figure 2.5 Fuel Cell Block

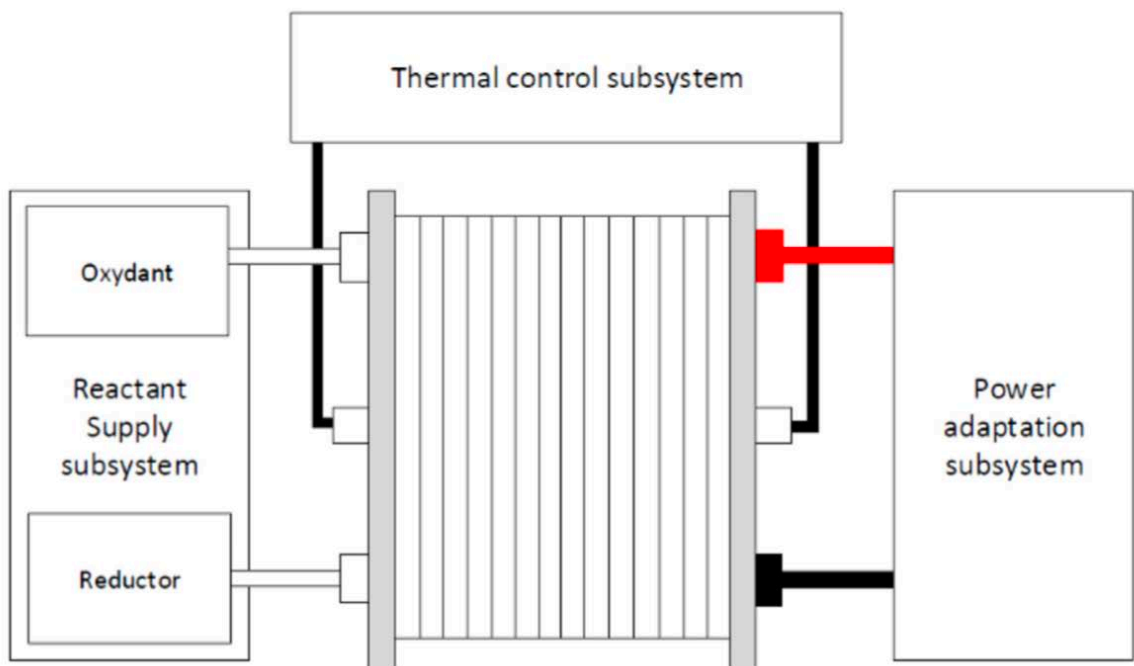


Figure 2.6 Fuel Cell System Components (Marx et al., 2017)

In this study, we will be assuming that all cells in the multi-stack are operating under the same conditions and at the same power generation rate. A fuel cell is a system that converts the chemical energy stored in the bonds between the two hydrogen cells into electric energy by oxidation-reduction reaction. The coproduct of this reaction

is water. This entails that this reaction does not emit any environmentally damaging gases or particles.

The problem with the fuel cell is that it has limited performance due to the transient load demand. Furthermore, the cost of the fuel cell system is still high compared to other power generating systems.

The parameters of an air-breathing fuel cell system composed of a stack from the manufacturer HORIZON (H-5000) and a power converter from ZAHN electronics (DC15036FSU) are considered in this thesis. Figure 2.4 is a realistic presentation of the H5000 multi stack of fuel cell. The fuel cell characteristics and specifications are all presented in table 2.2 and figures 2.7, 2.8, 2.9, 2.10

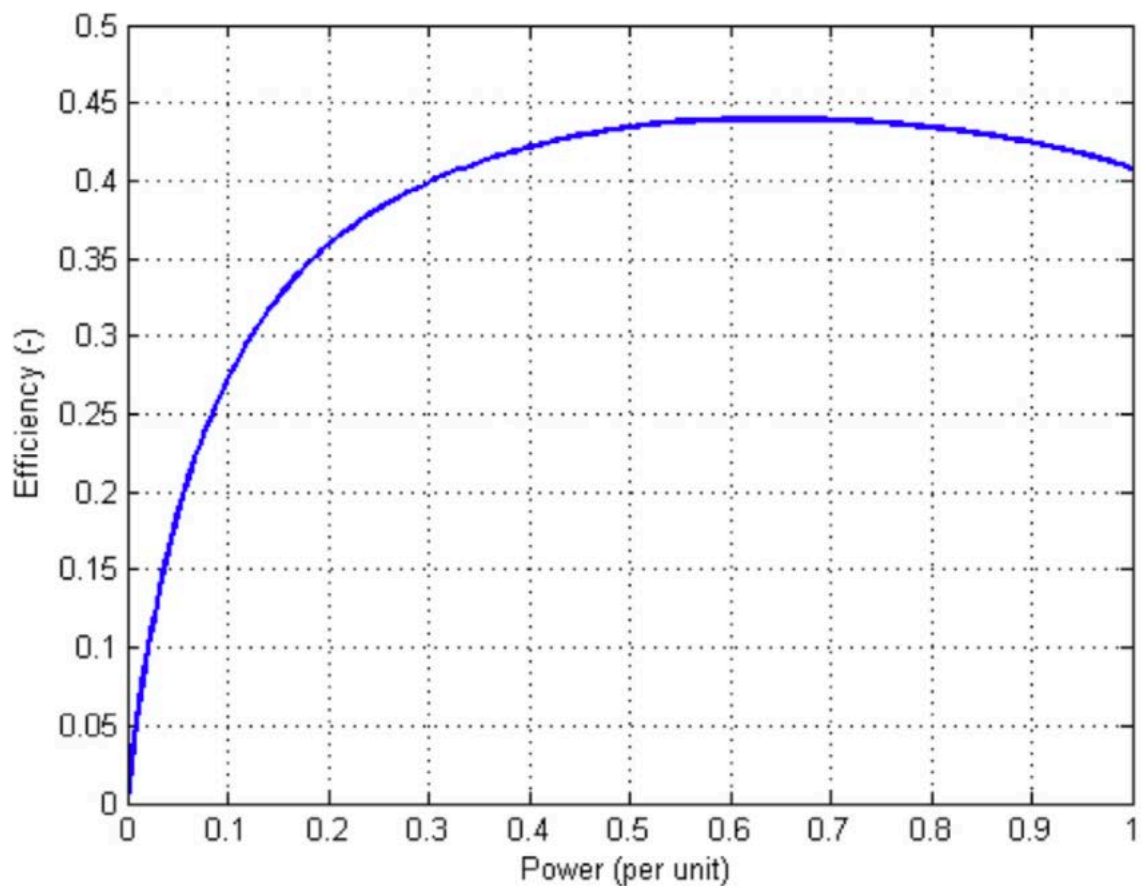


Figure 2.7 H5000 Efficiency Curve (Marx et al., 2017)

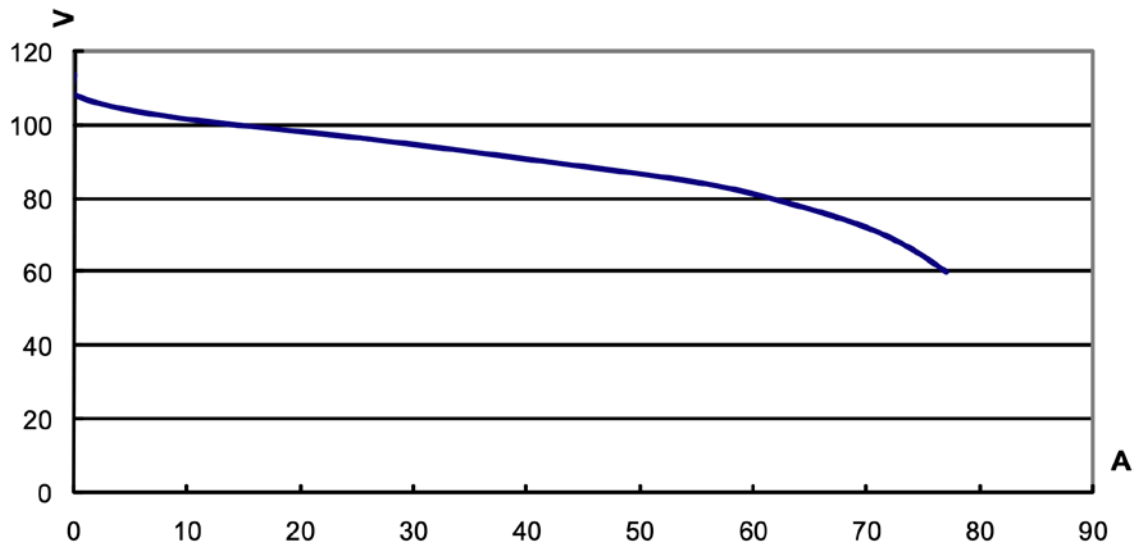


Figure 2.8 H5000 Voltage-Current Curve (Store, 2013)

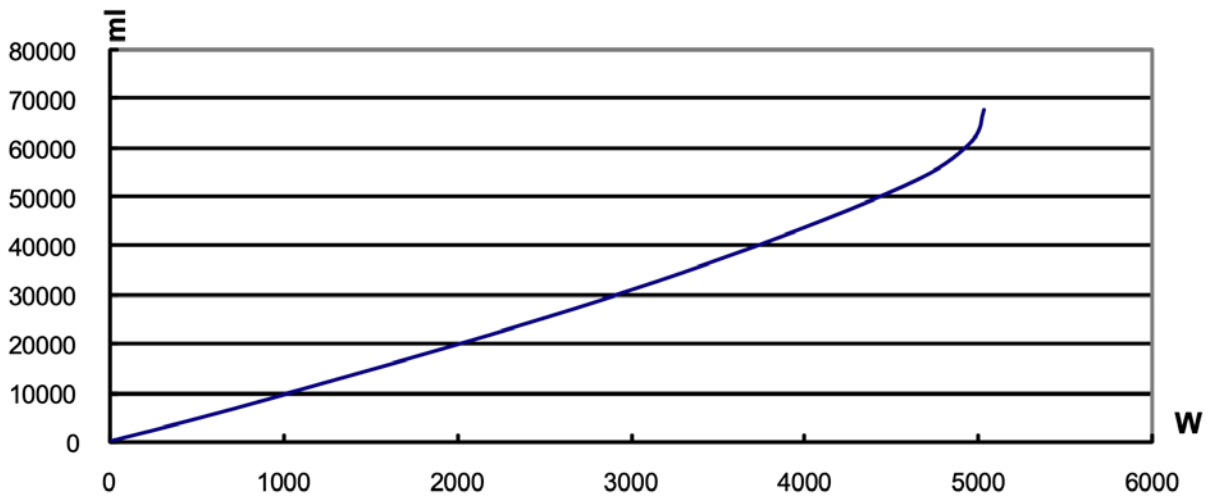


Figure 2.9 H5000 Hydrogen Consumption Curve (Store, 2013)

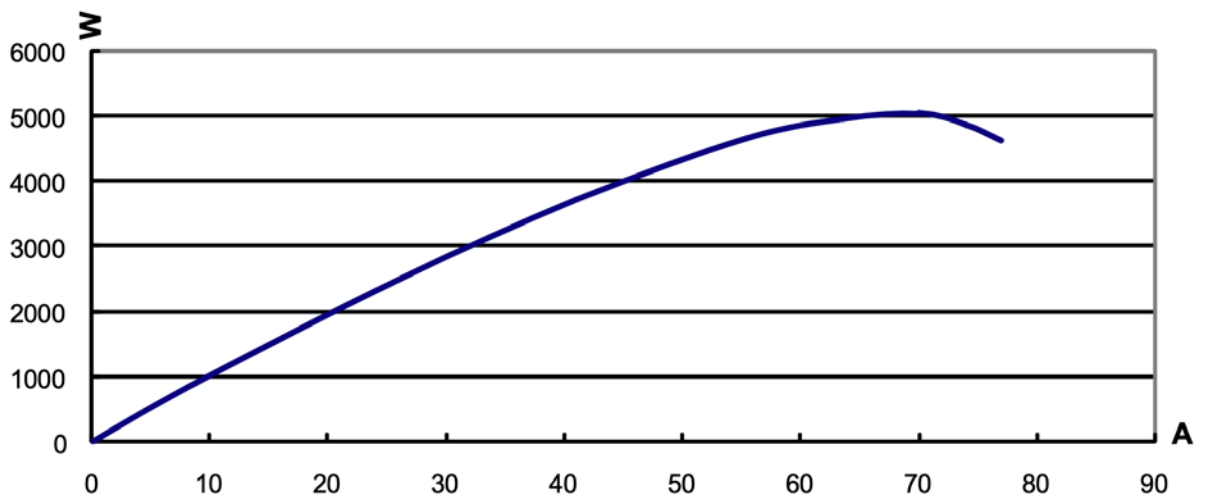


Figure 2.10 H5000 Power-Current Curve (Store, 2013)

The fuel cell will be modeled as an ideal voltage source with an internal resistance in series as shown in figure 2.11

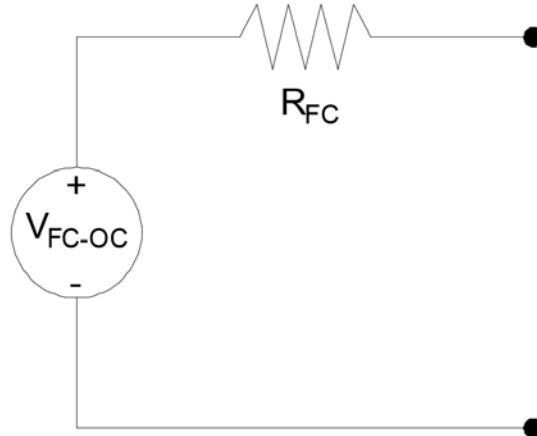


Figure 2.11 Fuel Cell Equivalent Circuit Model

The open circuit voltage of the fuel cell can be presented as shown in the equation (2.8)

$$V_{FC} = V_{FC0} - I_{FC}R_{FC} \quad (2.8)$$

P_{FC} is the power delivered by the fuel cell at its terminals, and it is directly related to the current of the fuel cell stack I_{FC} as shown in equation (2.9)

$$P_{FC} = V_{FC}I_{FC} = V_{FC0}I_{FC} - I_{FC}^2R_{FC} \quad (2.9)$$

This implies that the fuel cell stack current will be as follows:

$$I_{FC} = \frac{V_{FC0}}{2R_{FC}} \left(1 - \sqrt{1 - 4P_{FC} \frac{R_{FC}}{V_{FC0}^2}} \right) \quad (2.10)$$

The fuel consumption of a fuel cell is directly related to its current. Each molecule of hydrogen delivers two electrons. Thus, the hydrogen mass flow (\dot{m}_{H_2}) is proportional to the stack current, and it is presented in the equation below.

$$\dot{m}_{H_2} = \frac{N_{FC} M_{H_2}}{2F} I_{FC} = \frac{N_{FC} M_{H_2}}{2F} \frac{V_{FC0}}{2R_{FC}} \left(1 - \sqrt{1 - 4P_{FC} \frac{R_{FC}}{V_{FC0}^2}}\right) \quad (2.11)$$

M_{H_2} is the molar weight of hydrogen and F is the Faraday's constant.

Upper and lower limits bound the power supplied by a fuel cell:

$$P_{FCmin} \leq P_{FC} \leq P_{FCmax} \quad (2.12)$$

P_{FCmin} and P_{FCmax} usually represent the minimum and maximum rated operation powers of the fuel cell stack.

Type of fuel cell	PEM
Number of cells	120
Rated Power	5000W
Performance	72V @ 70A
H2 Supply valve voltage	12V
Purging valve voltage	12V
Blower voltage	24V
Reactants	Hydrogen and Air
External temperature	5 to 30°C
Max stack temperature	65°C
H2 Pressure	0.45-0.55bar
Hydrogen purity	$\geq 99.995\%$ dry H2
Humidification	self-humidified
Cooling	Air (integrated cooling fan)
Weight (with fan & casing)	30kg ($\pm 200g$)
Controller	2.5kg ($\pm 100g$)
Dimension	65cm x 35cm x 21.2cm
Flow rate at max output*	65 L/min
Startup time	$\leq 30S$ at ambient temperature
Efficiency of stack	40% @ 72V
Low voltage shut down	60V

Over current shut down	90A
Over temperature shut down	65 °C
External power supply	24V(±1V), 8A~12A

Table 2.2 H5000 Fuel Cell Characteristics

The cost of the fuel cell is 50 \$/kw and is expected to decrease in the future. Assuming a service life of 5000 hours, the service life cost of the fuel cell in \$/kwh becomes:

$$\gamma_{SL-FC} = 0.01 \text{ \$/kWh}$$

In addition to the service life cost of the fuel cell, the cost of hydrogen consumption is taken into account. The hydrogen is consumed by the fuel at a rate of 0.016 grams per kW. And the cost of hydrogen currently in the market is 14 \$/kg.

2.5 Battery Selection and System Model

The energy storage system model used in this thesis is a battery. The battery is the secondary source of energy in the FCHV. It is a bi-directional source as it supplies energy when demanded and stores the energy regenerated when the vehicle is using the brakes.

The battery is more responsive, than the fuel cell, to power demand fluctuations. It smoothens the demand on the fuel cell which helps in elongating the fuel cell life. There are many types of batteries available in the market such as Lead-based, Nickel-based and Lithium-based. They are presented in table 2.3. The type of battery most suitable for the automotive application is the Lithium-based battery because, although they are still very expensive, they have a high energy density, high power density and high charging/discharging efficiency ranging between 80 and 90%. With the increasing market production volume of Lithium-based batteries, the price is expected to significantly decrease in the coming decade.

A lithium ion battery is composed of an anode, a cathode, and an electrolyte membrane that allows the flow of ions between the two electrodes.

The battery is represented as an ideal voltage source with internal resistance as sketched in figure 2.12

The voltage at the terminal of the battery will be:

$$V_s = V_{s0} - I_s R_s \quad (2.13)$$

When the battery is being discharged, the power supplied at the terminals of the battery will be equal to the power from the ideal internal voltage source P_{s0} minus the internal losses over the resistor R_s .

$$P_s = V_s I_s - I_s^2 R_s = P_{s0} - P_{s0}^2 \frac{R_s}{V_{s0}^2} \quad (2.14)$$

The battery power is limited by upper and lower limits which are P_{\max} and P_{\min} .

$$P_{\min} \leq P_s \leq P_{\max} \quad (2.15)$$

When the battery is being charged, the values of the powers will become negative. So, the amount of energy stored in the battery will be referred to as the SOC. The SOC of the battery is directly related to the integral of the battery current.

$$\text{SOC}(t) = \text{SOC}(0) - \frac{1}{C_{s\max}} \int_{T=0}^t I_s dT \quad (2.16)$$

$C_{s\max}$ represents the battery's capacity to store charge. The minus sign in equation (2.16) is due to the definition of a positive battery current when discharging. SOC ranges between 0% and 100% but most manufacturers prescribe a safety range of allowable values:

$$\text{SOC}_{\min} \leq \text{SOC} \leq \text{SOC}_{\max} \quad (2.17)$$

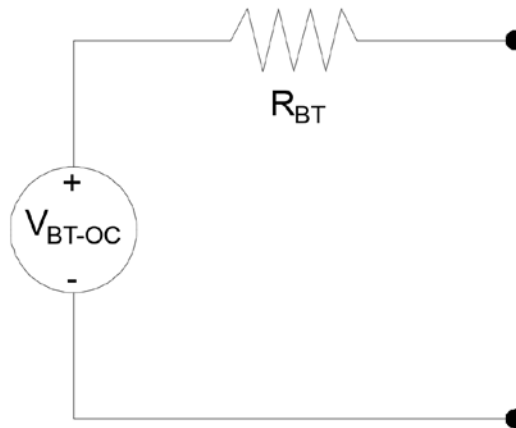


Figure 2.12 Battery Equivalent Circuit Model

Chemistry	Lithium Cobalt Oxide	Lithium Manganese Oxide	Lithium Nickel Manganese	Lithium Iron Phosphate	Lithium Nickel Cobalt Aluminum Oxide	Lithium Titanate
Short form	Li-cobalt	Li-manganese	NMC	Li-phosphate	Li-aluminum	Li-titanate
Abbreviation	LiCoC ₂ (LCO)	LiMn ₂ O ₄ (LMO)	LiNiMnCoO ₂ (NMC)	LiFePo ₄ (LFP)	LiNiCoAlO ₂ (NCA)	Li ₂ TiO ₃ (LTO)
Nominal voltage	3.60V	3.70V (3.80V)	3.60V (3.70V)	3.20, 3.30V	3.60V	2.40V
Full charge	4.20V	4.20V	4.20V (or higher)	3.65V	4.20V	2.85V
Full discharge	3.00V	3.00V	3.00V	2.50V	3.00V	1.80V
Minimal voltage	2.50V	2.50V	2.50V	2.00V	2.50V	1.50V (est.)
Specific Energy	150–200Wh/kg	100–150Wh/kg	150–220Wh/kg	90–120Wh/kg	200-260Wh/kg	70–80Wh/kg
Charge rate	0.7–1C (3h)	0.7–1C (3h)	0.7–1C (3h)	1C (3h)	1C	1C (5C max)
Discharge rate	1C (1h)	1C, 10C possible	1–2C	1C (25C pulse)	1C	10C possible
Cycle life (ideal)	500–1000	300–700	1000–2000	1000–2000	500	3,000–7,000
Thermal runaway	150°C (higher when empty)	250°C (higher when empty)	210°C (higher when empty)	270°C (safe at full charge)	150°C (higher when empty)	One of safest Li-ion batteries
Maintenance	Keep cool; store partially charged; prevent full charge cycles, use moderate charge and discharge currents					
Packaging (typical)	18650, prismatic and pouch cell	prismatic	18650, prismatic and pouch cell	26650, prismatic	18650	prismatic
History	1991 (Sony)	1996	2008	1996	1999	2008
Applications	Mobile phones, tablets, laptops, cameras	Power tools, medical devices, powertrains	E-bikes, medical devices, EVs, industrial	Stationary with high currents and endurance	Medical, industrial, EV (Tesla)	UPS, EV, solar street lighting

Comments	High energy, limited power. Market share has stabilized.	High power, less capacity; safer than Li-cobalt; often mixed with NMC to improve performance.	High capacity and high power. Market share is increasing. Also NCM, CMN, MNC, MCN	Flat discharge voltage, high power low capacity, very safe; elevated self-discharge.	Highest capacity with moderate power. Similar to Li-cobalt.	Long life, fast charge, wide temperature range and safe. Low capacity, expensive.
----------	--	---	---	--	---	---

Table 2.3 Lithium Base Battery Properties (Battery Univeristy, 2016, July 21)

Lithium Nickel Manganese Cobalt Oxide: LiNiMnCoO ₂ . cathode, graphite anode	
Short form: NMC (NCM, CMN, CNM, MNC, MCN similar with different metal combinations) Since 2008	
Voltages	3.60V, 3.70V nominal; typical operating range 3.0–4.2V/cell, or higher
Specific energy (capacity)	150–220Wh/kg
Charge (C-rate)	0.7–1C, charges to 4.20V, some go to 4.30V; 3h charge typical. Charge current above 1C shortens battery life.
Discharge (C-rate)	1C; 2C possible on some cells; 2.50V cut-off
Cycle life	1000–2000 (related to depth of discharge, temperature)
Thermal runaway	210°C (410°F) typical. High charge promotes thermal runaway
Cost	~\$420 per kWh (Source: RWTH, Aachen)
Applications	E-bikes, medical devices, EVs, industrial
Comments	Provides high capacity and high power. Serves as Hybrid Cell. Favorite chemistry for many uses; market share is increasing.

Table 2.4 Lithium Nickel Manganese Cobalt Oxide Cell Properties (Battery Univeristy, 2016, July 21)

Lithium Nickel Cobalt Aluminum Oxide: LiNiCoAlO ₂ cathode (~9% Co), graphite anode	
Short form: NCA or Li-aluminum Since 1999	
Voltages	3.60V nominal; typical operating range 3.0–4.2V/cell
Specific energy (capacity)	200-260Wh/kg; 300Wh/kg predictable
Charge (C-rate)	0.7C, charges to 4.20V (most cells), 3h charge typical, fast charge possible with some cells
Discharge (C-rate)	1C typical; 3.00V cut-off; high discharge rate shortens battery life

Cycle life	500 (related to depth of discharge, temperature)
Thermal runaway	150°C (302°F) typical, High charge promotes thermal runaway
Cost	~\$350 per kWh (Source: RWTH, Aachen)
Applications	Medical devices, industrial, electric powertrain (Tesla)
Comments	Shares similarities with Li-cobalt. Serves as Energy Cell.

Table 2.5 Lithium Nickel Cobalt Aluminum Oxide Cell Properties (Battery Univeristy, 2018, May 31)

Lithium Titanate: Can be lithium manganese oxide or NMC; $\text{Li}_4\text{Ti}_5\text{O}_{12}$ (titanate) anode	
Short form: LTO or Li-titanate Commercially available since about 2008.	
Voltages	2.40V nominal; typical operating range 1.8–2.85V/cell
Specific energy (capacity)	50–80Wh/kg
Charge (C-rate)	1C typical; 5C maximum, charges to 2.85V
Discharge (C-rate)	10C possible, 30C 5s pulse; 1.80V cut-off on LCO/LTO
Cycle life	3,000–7,000
Thermal runaway	One of safest Li-ion batteries
Cost	~\$1,005 per kWh (Source: RWTH, Aachen)
Applications	UPS, electric powertrain (Mitsubishi i-MiEV, Honda Fit EV), solar-powered street lighting
Comments	Long life, fast charge, wide temperature range but low specific energy and expensive. Among safest Li-ion batteries.

Table 2.6 Lithium Titanate Cell Properties (Battery Univeristy, 2018, May 31)

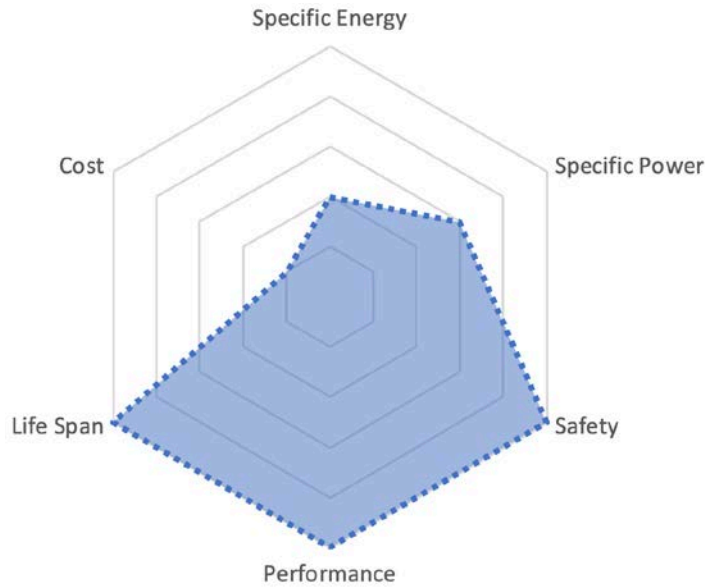


Table 2.7 Lithium Titanate Battery Properties Chart (Battery Univeristy, 2018, May 31)

For the FCHV application, battery power density is what matters the most, unlike electric vehicles (where large energy storage is required). However, as we need high power to be available, the batteries are sometimes oversized from an energy capacity perspective. Tables 2.4, 2.5, and 2.6 show the characteristics of the most suitable battery cells for automotive application.

Lithium Titanate might be the most suitable battery for this study for many reasons: It has the highest discharge rate (30C up to 5 seconds), the longest cycle life (3000-7000) and it is the safest Li-ion battery in the market. The only disadvantage is the high investment costs (1,005 \$/kWh). But if this cost is divided over the life cycles and the wattage of the battery it becomes:

$$\gamma_{BT} = \frac{1005}{5000} = 0.201 \$/kWh \quad (2.18)$$

In a FCHV, the battery also supplies power to the fuel cell subsystems and to the other auxiliaries available in the vehicle.

2.6 Electric Motor

The motor is what converts the electric energy to kinetic energy and drives the vehicle. It is supplied with power from the primary and secondary sources of energy and supplies enough mechanical power to meet the drive train torque and velocity requirements. Induction motor is mainly used for the automotive application.

In every electric motor we have power losses affecting its efficiency. These losses vary with the torque and rotational speed of the motor. The efficiency of the motor is modeled in a power map prepared by the supplier. Figure 2.14 is a sample efficiency map of the MC_AC124_EV1 obtained from the advanced vehicle simulator ADVISOR developed by the national renewable energy laboratory (NREL).

The size of the electric motor should be carefully chosen to meet the minimum drivability constraints of the vehicle, mainly the maximum acceleration requirement.

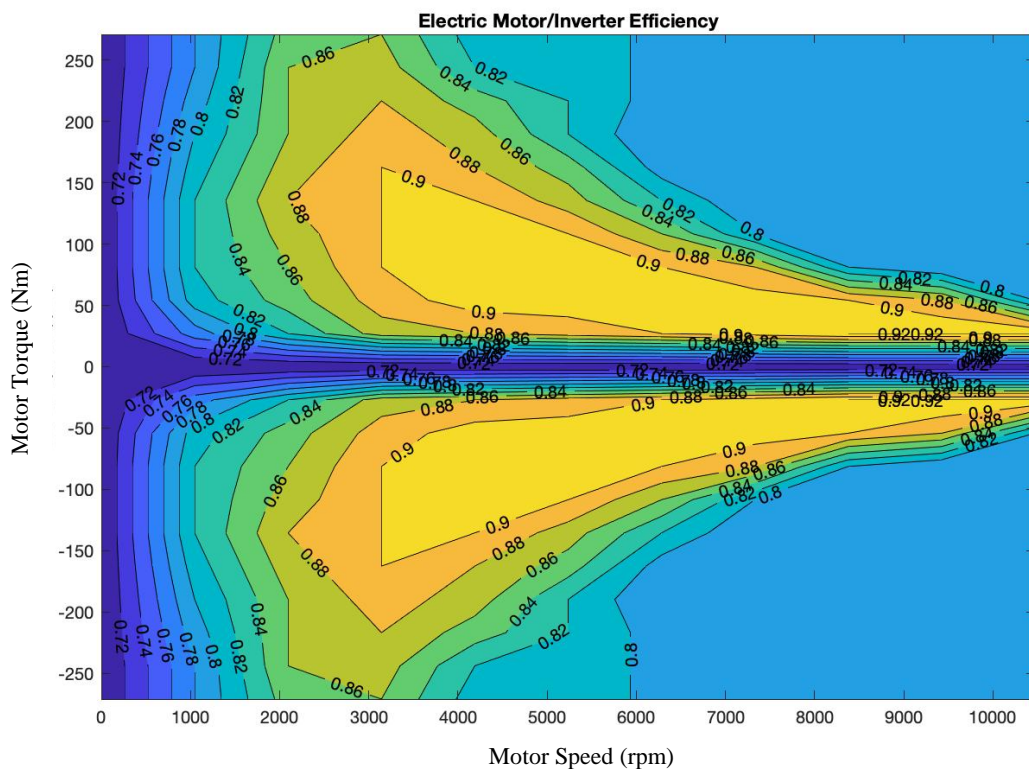


Figure 2.13 MC_AC124_EV1 Motor Efficiency Map

2.7 Transmission

The transmission system transmits the motor torque and rotational speed to the wheels. These output values are changed depending on the gear ratio of the system. Unlike vehicles powered by internal combustion engines, the FCHV transmission system has only one gear ratio that is designed based on the vehicle parameters and drivability requirements. The power losses in the transmission system are caused by the friction between the gears and their inertia.

The output rotation speed from the transmission system is modeled in the equation below:

$$w_w = \frac{w_m}{g_r} \quad (2.19)$$

The torque transmitted to the wheels is expressed as a function of the torque generated by the motor in the equation below:

$$\tau_{wheels} = g_r \tau_m - \frac{P_{Tloss}}{w_w} \quad (2.20)$$

Where P_{Tloss} represents the power loss in the transmission system.

2.8 Auxiliaries

In addition to the power required by the electric motor, there are other power consumers in the FCHV which are: the air conditioning system (600 watts), the power steering system (120 watts), the auxiliaries of the fuel cell (1000 watts), the lighting system (20 watts) and others. All these are shown in figure 2.15 and taken into account in the calculation and represented by P_{aux} .

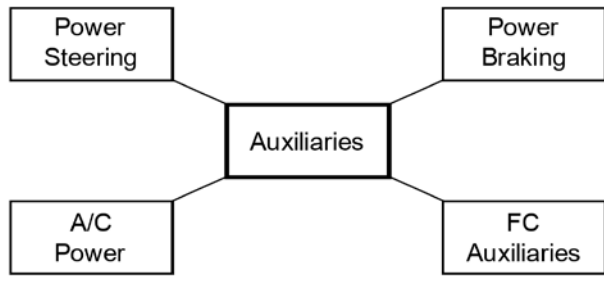


Figure 2.14 FCHEV Main Auxiliaries

CHAPTER 3

DRIVING CYCLES

Driving cycles are mainly used by the vehicle manufacturers and researchers to test the vehicle fuel consumption and polluting emissions. They are produced by organizations from different countries by gathering statistics about the driving habits of the drivers. Each driving cycle is a set of data representing the speeds of the vehicle on a defined time range. The driving cycles considered in this study are the Highway, FUDS, and NEDC. Each of these have a different profile, average speed, duration and distance.

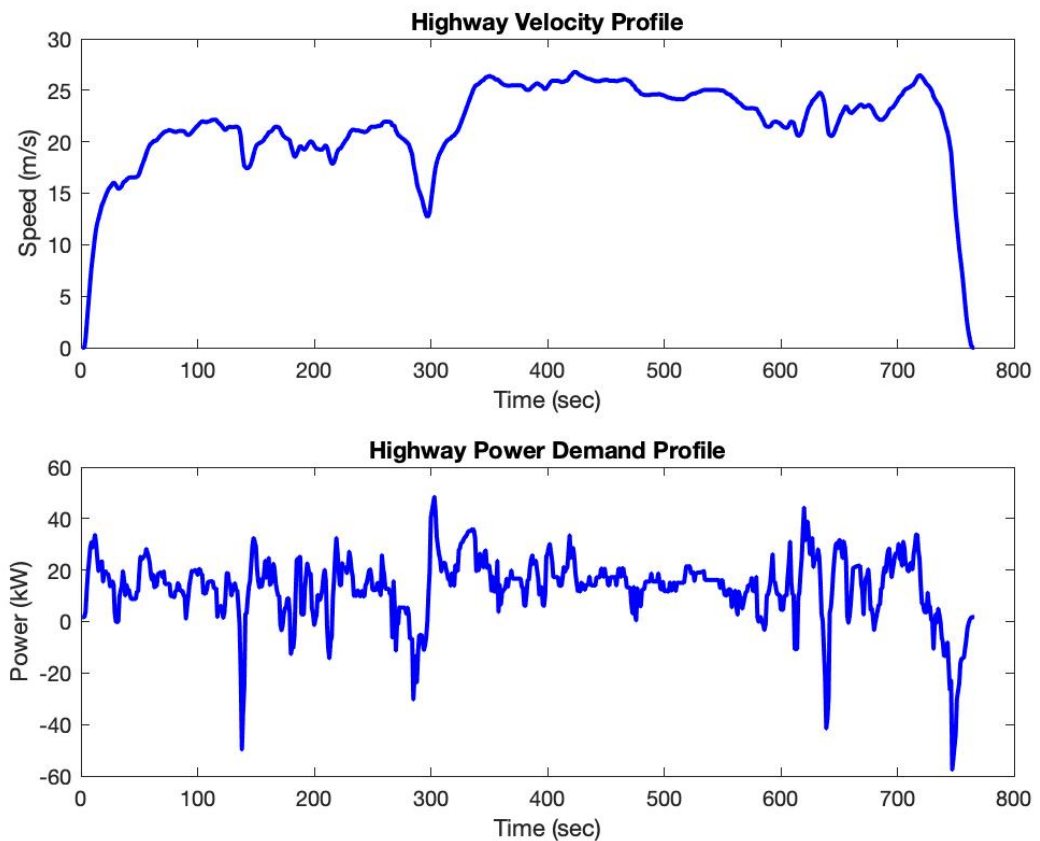


Figure 3.1 Highway Driving Cycle Speed and Demand Power Profiles

Figure 3.1 represents the speed and power demand profiles of the highway driving cycle. The highway driving cycle has a high acceleration at the start followed by high driving speeds ranging between 15 and 25 m/s and ends by a high deceleration. This driving is continuous until the driving cycle ends.

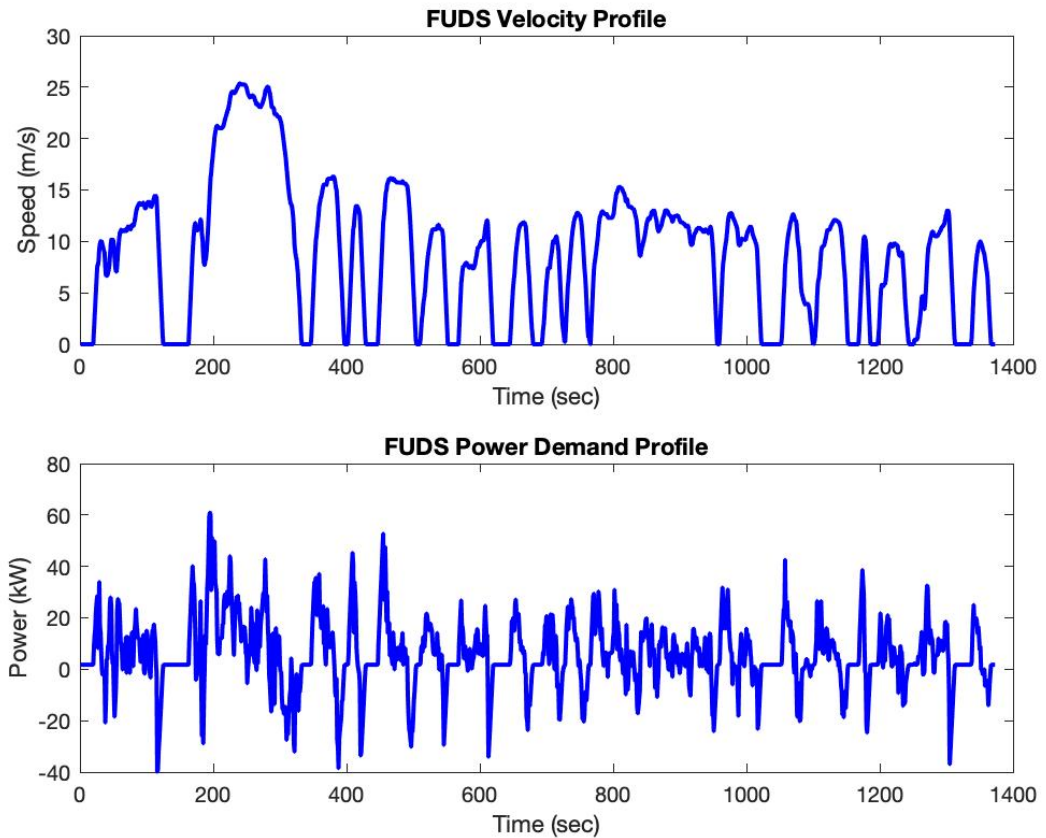


Figure 3.2 FUDS Driving Cycle Speed and Demand Power Profiles

Figure 3.2 represents the speed and power demand profiles of the Federal Urban Driving Schedule driving cycle. The FUDS has a higher acceleration and deceleration values compared to the highway, and it includes many stop/start patterns with different durations.

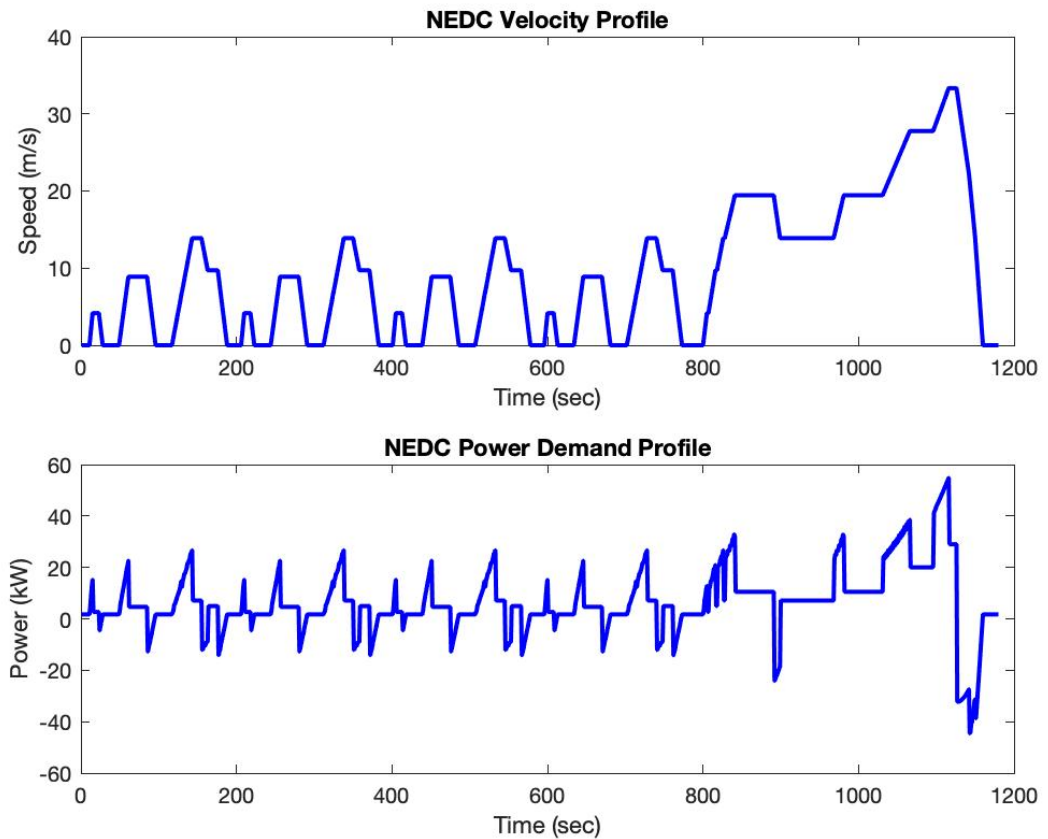


Figure 3.3 NEDC Driving Cycle Speed and Demand Power Profiles

Figure 3.3 represents the speed and power demand profiles of the National European Driving Cycle. It consists of an urban driving part repeated four times followed by an extra urban driving part. The maximum acceleration and decelerations are smaller than those of FUDS. The driving is interrupted by several stop/start patterns for long durations. Table 3.1 shows the summary of all the driving cycles considered in this thesis.

Characteristics	Unit	HIGHWAY	FUDS	NEDC
Distance	km	16.5	12.0	10.9
Time	sec	766.0	1373.0	1180.0
Max Speed	km/h	96.4	91.3	120.0
Average Speed	km/h	77.6	31.4	33.4
Max Acceleration	m/s ²	5.0	6.4	3.8
Max Deceleration	m/s ²	-5.3	-5.5	-5.0

Table 3.1 Driving Cycles Characteristics Summaries

CHAPTER 4

PROBLEM DEFINITION

The main objective of this thesis is to find the optimal size of power sources in a FCHV for the aim of reducing operational cost. Two techniques are used to achieve this goal:

1. TDP for the optimization of the EMS.
2. Pareto front to find the optimal battery and fuel cell sizes.

These two optimization techniques are explained in detail in the next chapters. In addition to the sizing optimization, battery selection is chosen based on different parameters.

CHAPTER 5

ENERGY MANAGEMENT SYSTEM

The EMS is used to monitor all the components' data measurements, and it controls the power split between the fuel cell and the energy storage. It is connected to each component as shown in figure 5.1.

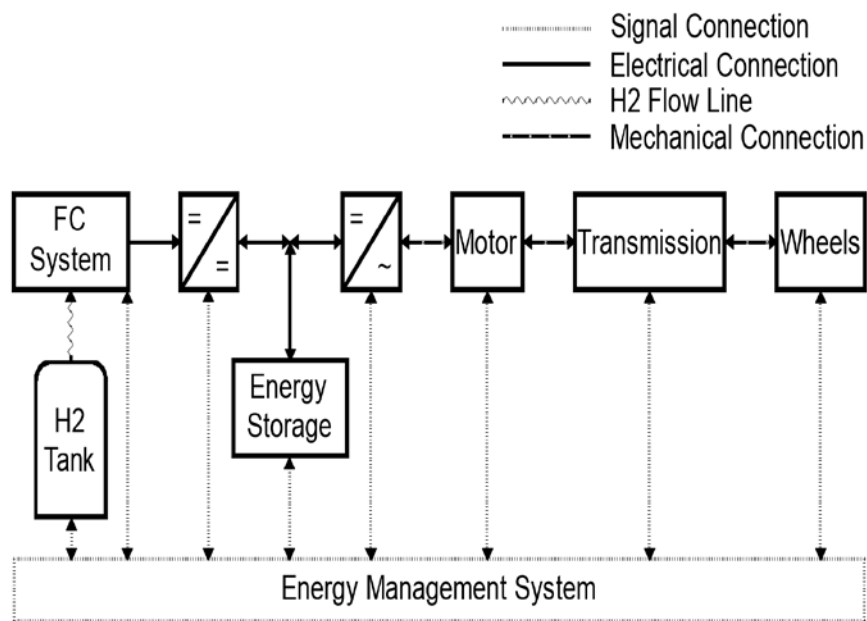


Figure 5.1 FCHV EMS

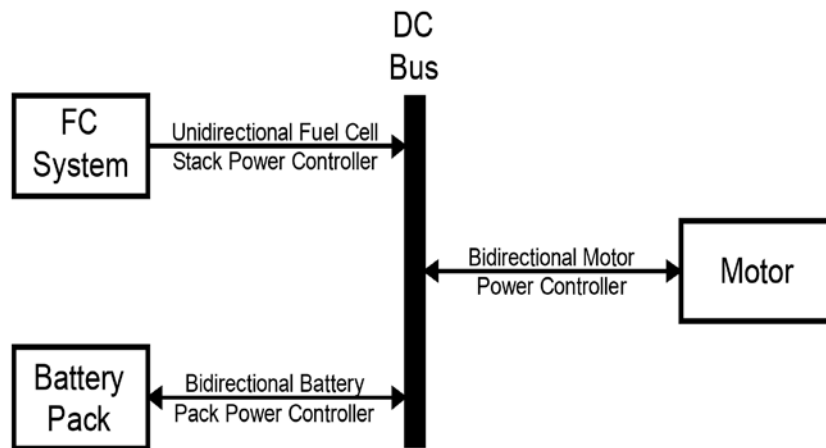


Figure 5.2 FCHV Electric Power Flow

Figure 5.2 shows the energy flow between the power sources and the electric motor. The power control is unidirectional for the fuel cell and bidirectional for the battery and the motor. The reason for using a bidirectional power controller is to enable the vehicle to capture the energy from regenerative braking. The amount of regenerative braking energy is significant, specifically in the driving cycles characterized by many stop/start patterns. This amount will be clearly presented in the results' chapter.

5.1 Tunnel Dynamic Programming for Optimum power Allocation

In the optimization method, the same methodology used by Fares et al. will be adopted to optimize the controller of a FCHV based on a TDP technique.

TDP is an enhanced version of DP through which the number of states at each time step is fixed. This enhancement eliminates the dimensionality problem of DP. In such a supervisory control model, an objective function along with the constraints are defined. The independent variables are defined through a set of actions while the dependent variables are defined in number states.

The time range is discretized into T steps that are equally distributed over the length of the driving cycle and it is presented on the horizontal axis. The number of states (S) is presented on the vertical axis. The state vector (u) is composed of fuel cell power levels that range from 0 to P_{FCmax} in equal steps. The figure 5.3, shows a model of the network with $S \times T$ interconnected nodes. This total number of nodes varies with the chosen number of states and time steps. Each node is given a certain index depending on its state and step numbers. N_{iuj} corresponds to the node at stage i and state u_j . All the nodes are characterized by a cost function C_{iuj} symbolized as nodal cost. So, C_{iuj} is the cost of being in the associated state. Starting from the second stage, each node will have an additional cost $R_{u_k, iuj}$. $R_{u_k, iuj}$ is the transition cost of moving from the previous state u_k at $i-1$ to the current state u_j at i .

F_{iuj} is the total cost associated with each node, and it is equal to the sum of the nodal cost and the minimum value of all transition costs to this node from the previous time step, as shown in equation 5.1.

Transition from a node at a certain time step to another node at the next time step should not defy any of the constraints mentioned later in this section (equation 5.7 to 5.14). If the transition is not acceptable, then it should be removed. An alternative way for removing it is by assigning a high transitional cost (100,000\$). The reason for using this alternative is to simplify the TDP MATLAB code. The simple code will converge faster than adding a complex technique of removing infeasible paths from the compounded multidimensional matrix. When a high cost is associated with a certain path, it will be very easy to take it out by lowest cost comparison at the end. At the end of the trip, when the last time step is executed, the lowest cost is marked and saved. The path of the lowest cost is traced back by to the initial time step and the optimal path will

be determined. Algorithm 5.1 shows how the code computes the costs and finds the cheapest operational cost path.

$$F_{iuj} = C_{iuj} + \min_k [R_{uk, iuj}] \quad \text{Where } i = 1:T \quad j, k = 1:S \quad (5.1)$$

$$\text{State Vector: } u = [u_1, u_2 \dots u_j \dots u_S] \quad \text{Where } j = 1:S$$

$$\text{State Vector: Stage} = [1, 2 \dots i \dots T] \quad \text{Where } i = 1:T$$

$$\text{Node Representation: } N_{iuj} \quad (5.2)$$

$$\text{Node Cost: } C_{iuj}$$

$$\text{Transition Cost: } R_{uk, iuj} \quad \text{Where } k = 1:S$$

Equation 5.2 represents all the terms used in equation 5.1.

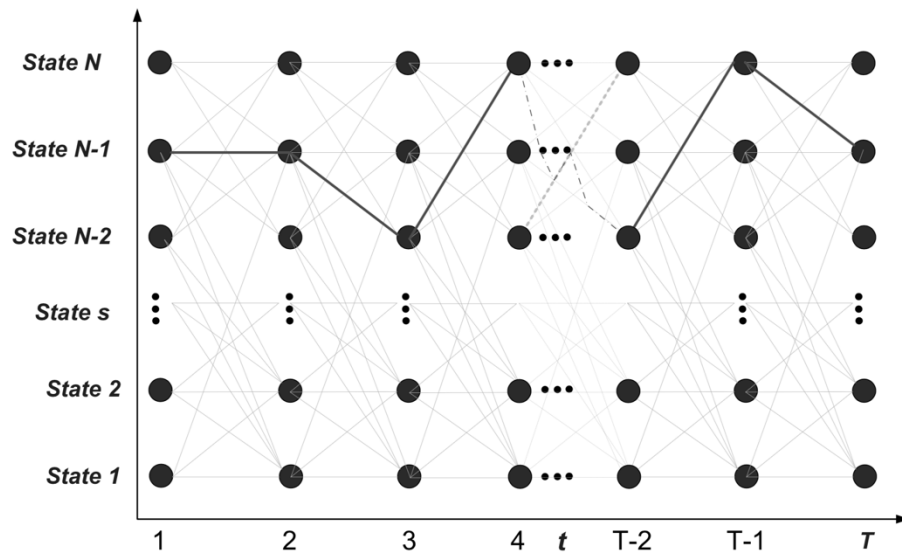


Figure 5.3 TDP Sketch

```

01: {Forward Path Generation}
02: for i such that i = 1 : T do
03:   for j such that j = 1 : S do
04:     for k such that k = 1 : S do
05:       Compute nodal cost  $C_{ij}$ 
06:       Compute transition cost  $R_{uk,ij}$ 
07:       Save index of min transition cost  $\text{Min} = [i, k_{\text{min}}]$  for min of  $R_{uk,ij}$ 
08:       Compute total cost  $F_{ij} = C_{ij} + R_{uk,ij} + C_{(i-1)uk}$ 
09:     end for
10:   end for
11: end for
12: {Backward Path Tracing}
13: for m such that m = 1 : T do
14:   Locate  $N(T) = \min(F_{Tij}) \forall j$ 
15:   Locate all  $N = \text{Min}(:,2)$ 
16: end for

```

Algorithm 5.1 TDP (Fares et al., 2015)

Algorithm 5.1 shows the forward path and the backward path tracing. The nodal cost is calculated at each state for each time step.

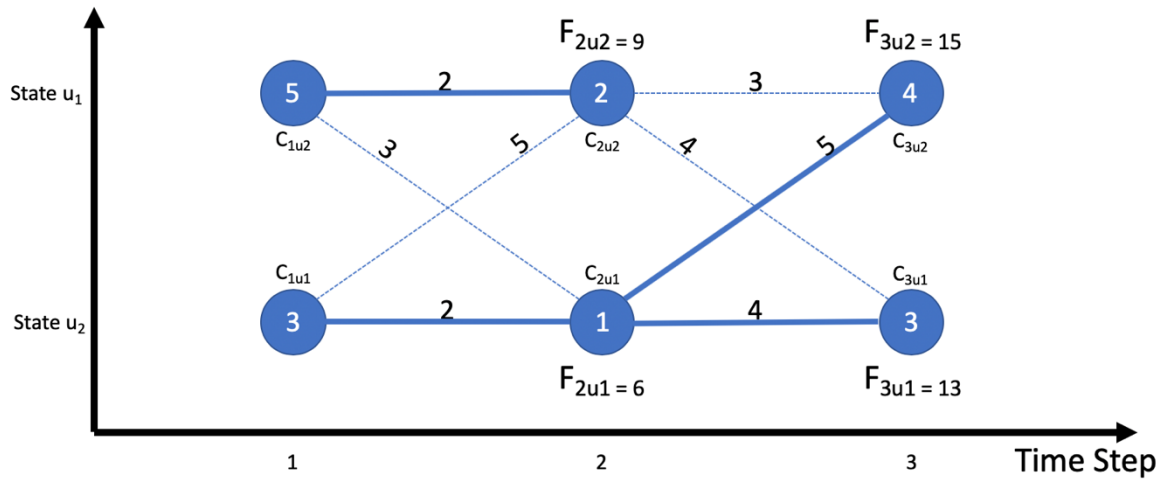


Figure 5.4 Example of TDP - Forward Path

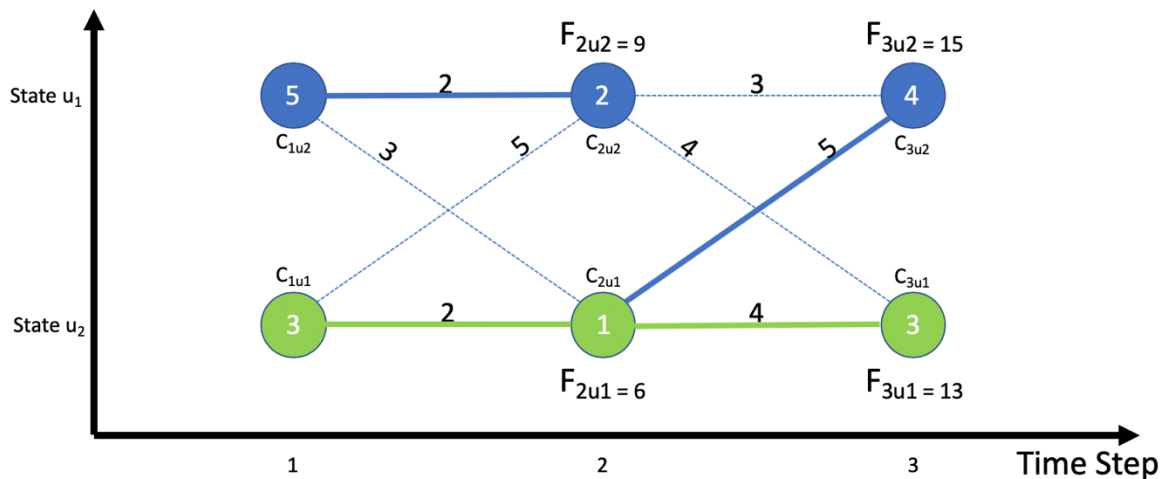


Figure 5.5 Example of TDP - Backward Path

To further explain this technique, an example model of 3 discrete time steps and 2 state levels is presented in figures 5.4 (forward path) and figure 5.5 (backward path). The total number of nodes is 6. Starting with the forward path, at $t = 1$, we have two different states u_1 and u_2 having two corresponding nodal costs $C_{1u1} = 3$ and $C_{1u2} = 5$. At $t = 2$, N_{2u1} can be reached either from node N_{1u1} or node N_{1u2} . The minimum total cost to reach this node is $F_{2u1} = 6$ from N_{1u1} as indicated by the blue line in figure 3.1. Similarly, the minimum cost to reach node N_{2u2} is $F_{2u2} = 9$ from N_{1u2} . It is also the same case for the 3rd time step ($t=3$). The minimum total costs F_{3u1} and F_{3u2} to reach nodes N_{3u1} and N_{3u2} , respectively, are associated with the transition from node N_{2u1} ; Therefore, $F_{3u1} = 13$ and $F_{3u2} = 15$. Finally, the minimum cost at $t=3$ is $F_{3u1} = 15$. For the backward path, F_{3u1} is selected and traced back to the first time step following minimum cost route. This route is shown in the green line in figure 5.5. If we use DP for this model, we will end up with fourteen nodes instead of six, which clearly explains why TDP is better than DP. TDP solves the dimensionality problem without drastically affecting the optimal path.

As per Fares et al., the nodal cost for the FCHV at each node is represented in the equation 3.3. (Fares et al., 2015)

$$C_{iu_j} = [(Y_{FC} + Y_{SL-FC})P_{FC,iu_j} + \frac{1}{2}Y_{BT}P_{BT,iu_j}] \quad (3.3)$$

Y_{FC} is the cost per kWh of the fuel cell consumption

Y_{SL-FC} is the service life cost per kWh of the fuel cell

Y_{BT} is the battery cost per kWh of the battery

P_{FC,iu_j} is the fuel cell power at the node iu_j

P_{BT,iu_j} is the battery power at the node iu_j

The battery's SOC must be updated at each time step. At the time the battery is discharging power and feeding the load, the battery power shows to be positive. Because of losses, the battery supplies less power to the load than what it actually discharges. On the other hand, the battery power is negative when the load is generative. The energy captured by the battery is smaller than that generated from the movement of the vehicle for the same reason which is the electromagnetic and transmission losses. Equation 5.4 shows how these losses are depicted in the calculation of the SOC at each step.

$$SOC_{iu_j} = \begin{cases} SOC_{(i-1)u_j} - \frac{P_{BT,iu_j}\Delta t}{\eta_{BT}C_{BT}} & \text{if } P_{BT,iu_j} \geq 0 \\ SOC_{(i-1)u_j} - \frac{\eta_{BT}P_{BT,iu_j}\Delta t}{C_{BT}} & \text{if } P_{BT,iu_j} < 0 \end{cases} \quad (5.4)$$

Equation 5.5 presents the power split during charging and discharging. This equation represents the feasibility of each state at each time step during the process.

$$P_{FC,iu_j} + P_{BT,iu_j} - P_{br,iu_j} = P_{L,i} \quad (5.5)$$

$P_{L,i}$ is the load power at time step i

P_{br,iu_j} is the regenerative braking power at node iu_j

To go from one node to the next, we consider the feasibility in terms of transitional cost. If the transition is feasible, then we consider a zero cost, while allocating an extremely high cost when it is infeasible.

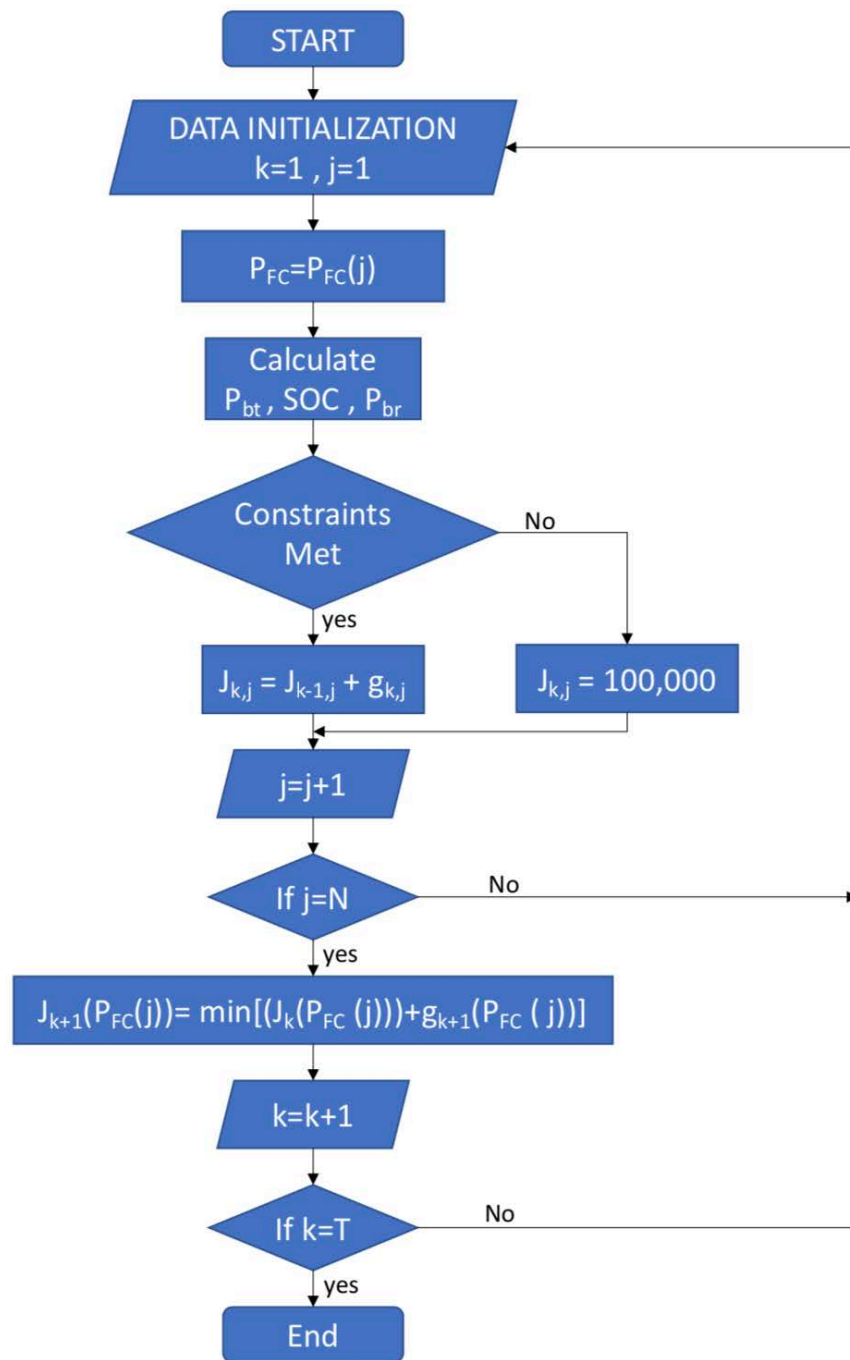


Figure 5.6 TDP Forward Algorithm (Fares et al., 2015)

The forward path of the TDP is graphically presented in figure 5.6. The iteration of the forward path ends when the time step T is reached. The costs at the last time step are compared and the node of the lowest cost is indexed. After that, the cheapest path is

traced back using backward path algorithm to the first time step and the optimal path is determined.

The objective function for the TDP is:

$$J = \min \left[\sum_{k=1}^N [(\gamma_{FC} + \gamma_{SL-FC})P_{FC}(k) + \gamma_{BT}P_{BT}(k)]\Delta t \right] \quad (5.6)$$

Below are the constraints that need to be taken into consideration during the solution of the optimization problem:

SOC Period Coupling Constraint

$$SOC(t) = SOC(t-1) - \frac{P_{BT}(t)\Delta t}{\eta_{BT}C_{BT}} \quad (5.7)$$

Power Balance Constraint

$$P_{FC}(t) + P_{BT}(t) - P_{br}(t) = P_L(t) \quad (5.8)$$

Fuel Cell Power Limits

$$P_{FCmin}(t) \leq P_{FT}(t) \leq P_{FCmax}(t) \quad (5.9)$$

Battery Power Limits

$$P_{BTmin}(t) \leq P_{BT}(t) \leq P_{BTmax}(t) \quad (5.10)$$

Battery SOC Limits

$$SOC_{min}(t) \leq SOC(t) \leq SOC_{max}(t) \quad (5.11)$$

FC Ramp Rate Constraint

$$R_{down-FC}\Delta t \leq P_{FC}(t) - P_{FC}(t - 1) \leq R_{up-FC}\Delta t \quad (5.12)$$

Battery Ramp Rate Constraint

$$R_{down-BT}\Delta t \leq P_{BT}(t) - P_{BT}(t - 1) \leq R_{up-BT}\Delta t \quad (5.13)$$

Hydrogen Tank Capacity Constraint

$$\sum_{k=1}^N \lambda P_{FC}(t)\Delta t \leq MH_0 \quad (5.14)$$

5.2 Operation Modes

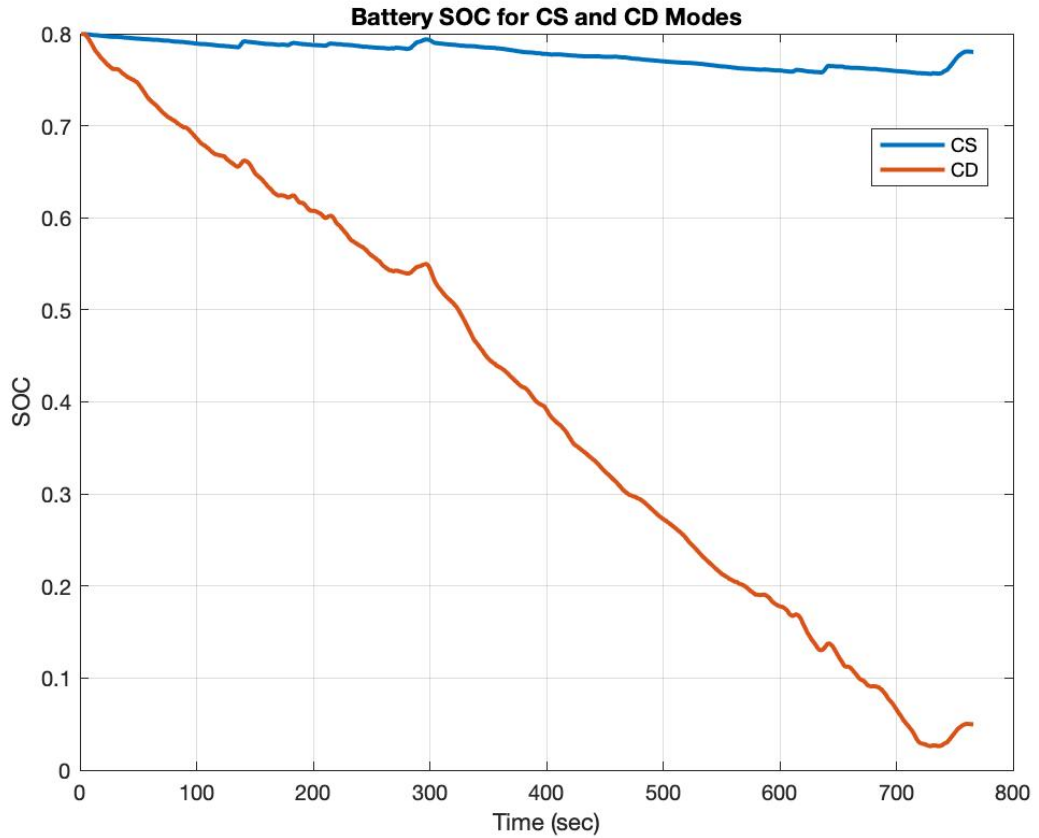


Figure 5.7 FCHV Operating Modes - CS & CD

The study will be performed on two operation modes for the EMS: The CD mode and the CS mode.

In CD mode, the EMS relies more on the battery which leads to the continuous reduction in the SOC of the battery. The fuel cell operates in two cases: when the battery gets fully depleted or when the demand power is higher than the battery power.

Since the cost of power supplied by the battery is cheaper than the power supplied by the fuel cell, the system will automatically operating in CD mode if no modifications are done to the objective function

In CS mode, the EMS relies more on the fuel cell. The battery only supplies power when the demand power is higher than the power capacity of the fuel cell.

The CS modes can be achieved by adding a weight to the cost of the battery only in the optimization function and not in the cost calculation. The aim is to make the battery look more expensive during the calculation which increases the reliance more on the fuel cell and thus keeping the SOC in the desired range (full range for the CD mode and +/- 5% for the CS mode)

The objective function becomes as shown in the equation below:

$$V_{iu_j} = ([(\gamma_{FC} + \gamma_{SL-FC})P_{FC,iu_j}] + \frac{1}{2} \omega_{BT}[\gamma_{BT}P_{BT,iu_j}])\Delta t \quad (5.15)$$

Where ω_{BT} is the weight added to the battery cost.

CHAPTER 6

POWER SOURCES SIZING OPTIMIZATION

6.1 Drivability Constraints

Before optimizing the size of the power sources in a HEV, minimum drivability constraints should be taken into consideration. There are three factors that determine the drivability of the vehicle: Maximum speed, gradeability and acceleration ability.

6.1.1 *Maximum Speed*

The speed ability of a vehicle is assessed on a 0% inclined road. The vehicle should be able to maintain a maximum constant speed of 150 km/h or 41 m/s with the fuel cell being the only source of power (Zheng et al., 2014). In other words, the fuel cell, which is the primary source of power, should be able to provide the necessary power for the motor to drive the car at the maximum speed without the need of the secondary source of power which is the battery. This constraint determines the minimum feasible power from the fuel cell. The reason we do not account for the battery as a source of power in this case is that for long distances on the highway, we might get to a point where the battery will reach its minimum allowable SOC, losing its ability to assist the fuel cell in supplying power to drive the motor.

So, the first constraint is: $P_{fc} > P_{fcmin1}$

To calculate P_{fcmin1} , we consider the vehicle parameters and the vehicle dynamic system explained in chapter 2.

The calculated minimum required power for the fuel cell to be able to solely drive the vehicle at a constant speed of 150 km/h or 41 m/s at a horizontal road is 34 kW.

6.1.2 Gradeability

The gradeability of a vehicle is assessed on a 5% (or 2.86°) inclined road. The vehicle should be able to maintain a maximum constant speed (110 km/h or 30.6 m/s) with the fuel cell being the only source of power (Zheng et al., 2014). The reason is the same as explained in the maximum speed section. The second constraint is: $P_{fc} > P_{fcmin2}$. We use the same data and models as explained in the maximum speed section, but we change the maximum speed and the inclination angle.

The calculated minimum required power for the fuel cell to be able to drive the vehicle solely at a constant speed of 110 km/h or 30.6 m/s at a 5% or 2.86° inclined road is 41 kW.

6.1.3 Acceleration

The acceleration is also a major constraint used to evaluate the drivability of the vehicle. The vehicle should be able to accelerate from 0 km/h to 100 km/h or 27.8 m/s in 12 seconds (Zheng et al., 2014). This constraint helps determine two parameters: the minimum size of the motor and the maximum required electric power. For the vehicle to comply with the above-mentioned requirement, the size of the motor should be large enough to provide the required mechanical power to the wheels. Unlike the maximum speed and gradeability constraints, the battery assists the fuel cell to provide the necessary power to accelerate. The fuel cell will not be able to supply the power alone, otherwise, a large fuel cell size is required.

Similarly to the maximum speed constraint, the acceleration ability is assessed on a 0% grade road.

The third constraint is $P_{\text{mot}} > P_{\text{motmin}}$, and the fourth constraint is:

$P_{\text{bat}} > P_{\text{mot}} / (N_{\text{mot}} * N_{\text{Trans}}) - P_{\text{fc}}$ where N_{mot} is the average efficiency of the motor in the motoring phase and N_{trans} is the average efficiency of the transmission system.

The same data and models used for the previous two constraints are also adopted for this constraint. Assuming that the vehicle speed is constantly increasing from 0 km/h to 100 km/h or (27.78 m/s) in 12 seconds as shown in figure 6.1, the value of the acceleration will be 2.315 m/s².

The result of the required power is shown in the figure 6.2 above. The more the velocity of the vehicle is increasing, the higher is the power required to achieve the desired acceleration. It keeps on increasing until it reaches a maximum value of $P_{\text{motmin}} = 123 \text{ kW}$.

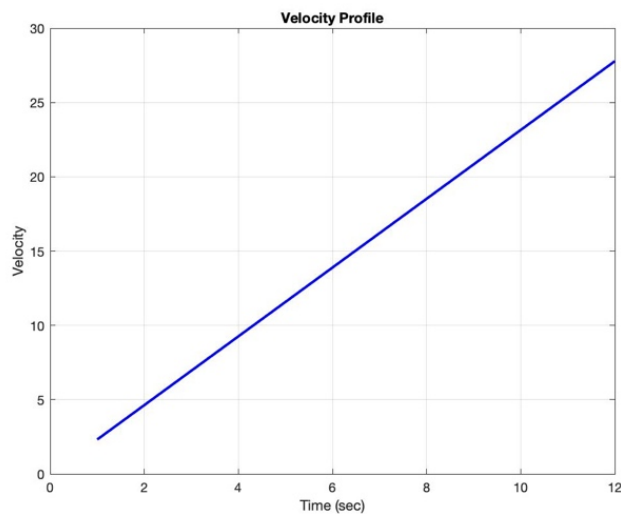


Figure 6.1 Vehicle Speed Profile for Maximum Acceleration Constraint

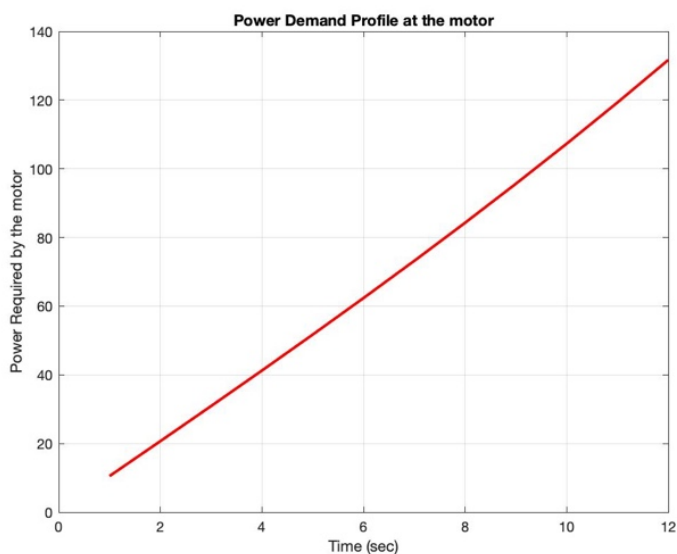


Figure 6.2 Power Demand for the Maximum Acceleration Constraint

6.1.4 Combined Constraints

The constraints that determine the minimum sizes of the fuel cell power sources are presented in the three previous sections. For the maximum speed constraint, the minimum power required from the fuel cell should be greater than 34 kW. As for the gradeability constraint, the minimum power required from the fuel cell should be greater than 41 kW. The final constraint shows that the value of power supplied by the two power sources combined should be more than 123 kW which is also the minimum size of the electric motor. MC_AC124_EV1 is an electric motor manufactured by general motors and its rated power is 124 kW.

Figure 6.3 below shows the region of the feasible power source sizes. All fuel cell sizes on the left of the red line won't be feasible for the gradeability of the vehicle and all the size combinations below the blue lines won't be enough for the required acceleration ability of the vehicle.

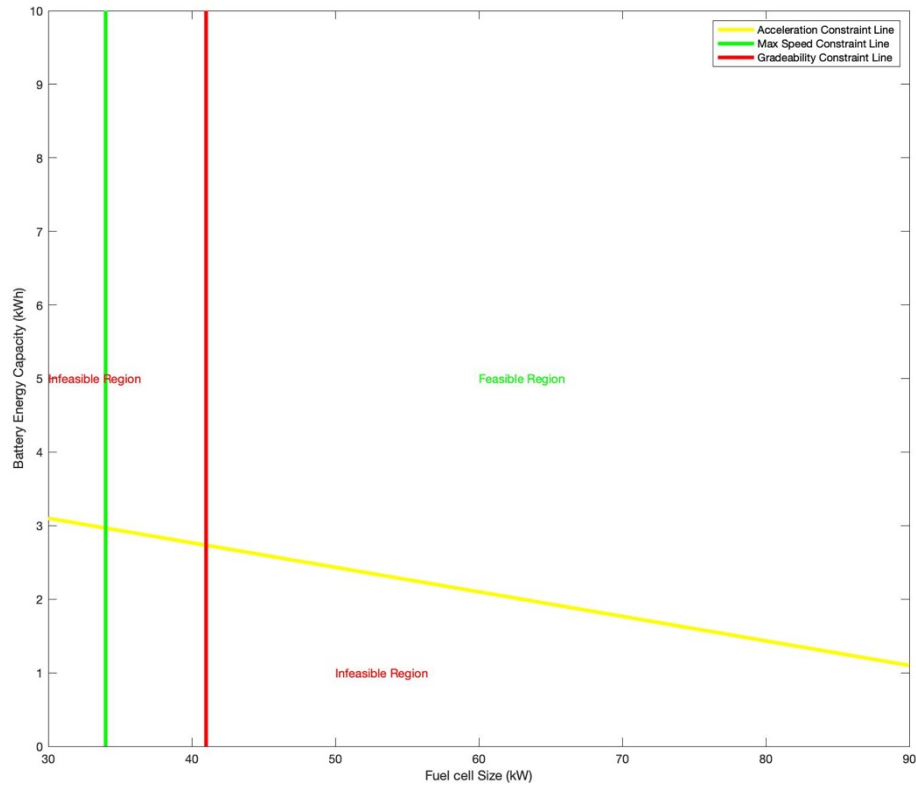


Figure 6.3 Combined Drivability Constraint Specifying the Feasible Region

6.2 Pareto Front

Pareto analysis is an adopted technique that serves to select a course of action when many courses of actions are possible. It therefore helps to define the optimal course of action being most beneficial amongst all the possible competing courses of action. Pareto analysis also helps to identify the ultimate best combination of tasks reaching best output or product, including quality control and many other applications.

As our target in this study is to find the optimal mix of batteries and fuel cells, with the least operational cost per trip for the three driving cycles, we selected different combinations of battery sizes and fuel cell stack sizes for analysis. To do so, algorithm

6.1 is used. In this algorithm, TDP is executed for every combination of fuel cells and batteries in a specific sizing range.

```
01: {Sizing Simulation}
02: Define battery sizes range vector
03: Define fuel cell sizes range vector
04: for every battery size do
05:     for every fuel cell size do
06:         for every driving cycle do
07:             Run TDP Algorithm
08:             Save the results
09:         end for
10:     end for
11: end for
12: Plot Results
```

Algorithm 6.1 Sizing Simulation Algorithm

The results of the simulation are presented in the next chapter.

CHAPTER 7

RESULTS

In this chapter, all the simulation results are presented. For each driving cycle, contour and regular plots are presented. For each driving mode per driving cycle, two plots are used.

The contour plot is used to show the level of operational cost against the variation of both the battery capacity and the power of the fuel cell. The battery capacity is presented on the Y-axis and the power of the fuel cell is presented on the X-axis. The color of the contour plot indicates the operational cost level. The color bar shown on the right side of the plot presents the values corresponding to each color. The red line inside the plot represents the maximum speed constraint. The yellow line inside the plot represents the maximum acceleration constraint. Any combination point that lies on the left of the red line or below the yellow line is infeasible and doesn't meet the minimum drivability constraints.

The regular plot also shows the variation in trip cost against the variation of the battery capacity for each power capacity of the fuel cell. The trip cost is presented on the Y-axis and the battery capacity is presented on the X-axis. Each color in the plot represents a fuel cell power capacity as shown in the legend in the upper right corner.

The EMS Using DP plot of each driving mode shows the power split for the two power sources. The Y-axis presents the power value and the X-axis presents the time value. The black dashed line presents the total power demand, the blue line presents the portion of power supplied by the fuel cell, and the red line presents the portion of power supplied by the battery. The Battery SOC Using DP plot shows the variation of the SOC of the battery during the trip. The Y-axis presents the percentage of the SOC and the X-axis presents the time value.

At the end of each driving mode, a table is used to present all the parameters and results for each driving mode belonging to its corresponding driving cycle.

7.1 Highway

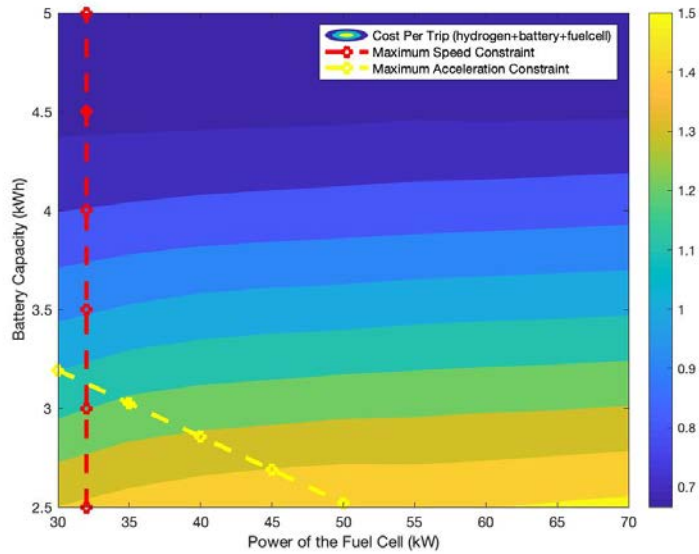


Figure 7.1 Trip Cost Contour Plot for Highway Driving Cycle

Figure 7.1 shows the contour plot of the sizing optimization on the highway. The optimal and feasible size combination for batterie capacity and fuel cell power is 4.5 kWh and 35 kW respectively.

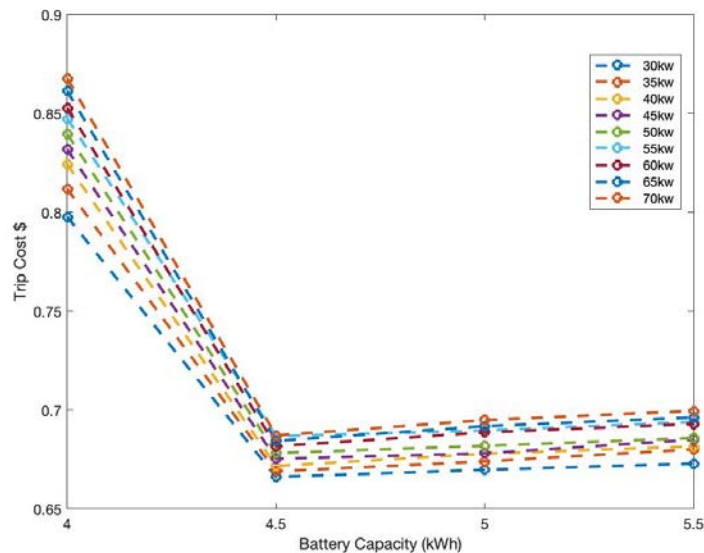


Figure 7.2 Pareto Front for Highway Driving Cycle

Figure 7.2 shows the resulting Pareto front which represents the best trade-off between the two conflicting objectives: reducing the trip cost vs. reducing the number of batteries for the different fuel cell power sizes. As per the plot in figure 7.2, the best

fuel cell size is 30 kw, but as per the contour plot in figure 7.1, this solution is not feasible.

7.1.1 CD Mode

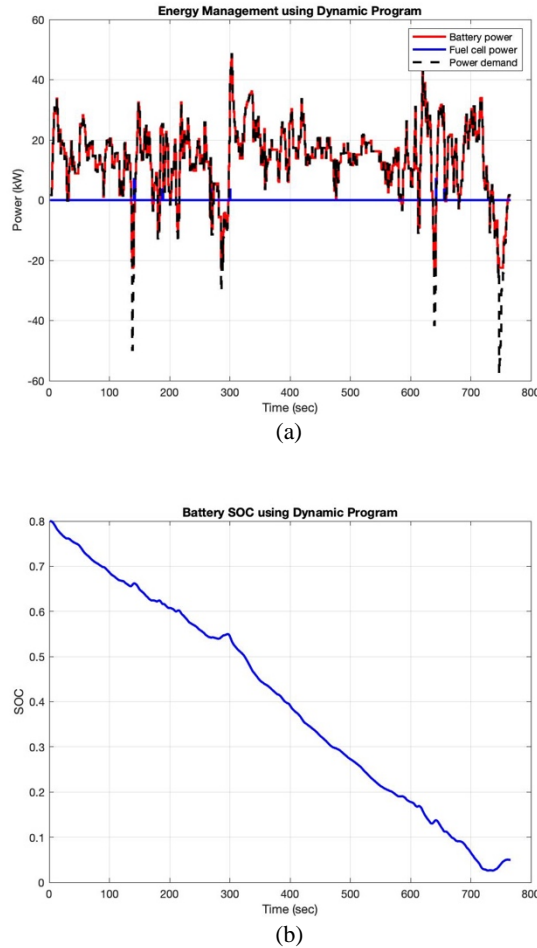


Figure 7.3 Power Allocation and SOC for CD Mode – Highway

As shown in figure 7.3, the operation mode is CD, the power is mainly supplied by the battery, and the battery keeps on depleting until the trip ends. The initial SOC was 80%, and the final SOC was approximately 4.9%. The total energy supplied by the battery is greater than the energy supplied by the fuel cell. The energy captured by the battery from regenerative braking is 7% of the total energy required for the trip. Table 7.1 presents all the variables and results of the trip simulation.

The Power of the Fuel Cell	35	kW
----------------------------	----	----

The Size of the Battery	4.5	kWh
Initial Stored Energy in The Batteries	3.6	kWh
The total system weight	2164.2857	kg
Total Energy Required for the trip	3.0974	kWh
Total Energy Supplied by the Fuel Cell	0.0077778	kWh
Total Energy Supplied by the Battery	3.0917	kWh
Total Energy Captured by the Battery	0.22162	kWh
Initial State of Charge (SOC0)	80	%
Final State of Charge (SOCF)	4.9656	%
Energy Difference from Initial Stored	3.9724	kWh
Distance Travelled	16.5061	km
Time of the Trip	766 (12.7667)	seconds (minutes)
Average Speed	77.5741	km/h
Cost of Operation	0.66901	\$
Total H2 Consumption	0.448	grams
The hydrogen consumption	0.0027142	kg / 100 km
The Current Tank Capacity Drives the Vehicle for	184219.3142	km

Table 7.1 Simulation Results for Highway in CD Mode

7.1.2 CS Mode

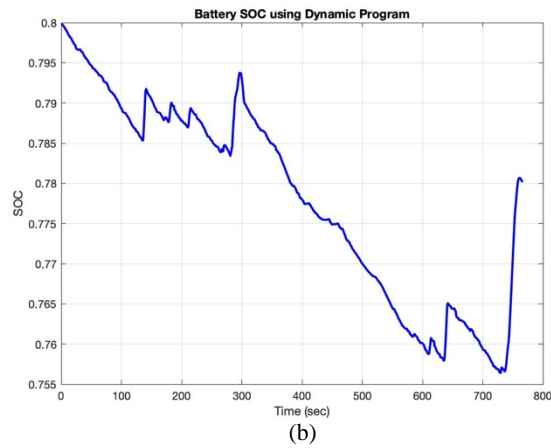
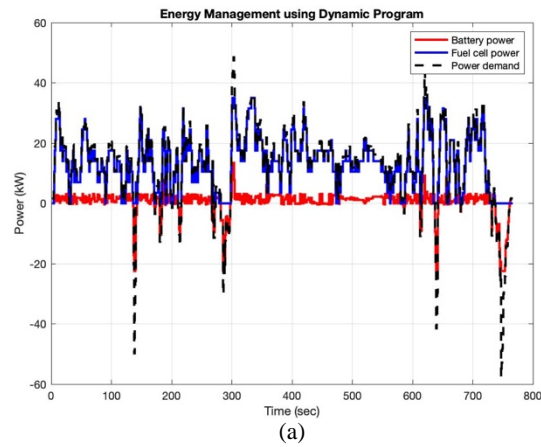


Figure 7.4 Power Allocation and SOC for CS Mode – Highway

As shown in figure 7.4, the operation mode is CS, the power is mainly supplied by the fuel cell. The initial SOC was 80% and the final SOC was approximately 78%.

Table 7.2 presents all the variables and results of the trip simulation.

The Power of the Fuel Cell	35	kW
The Size of the Battery	4.5	kWh
Initial Stored Energy in The Batteries	3.6	kWh
The total system weight	2164.2857	kg
Total Energy Required for the trip	3.0974	kWh
Total Energy Supplied by the Fuel Cell	2.8019	kWh
Total Energy Supplied by the Battery	0.30081	kWh
Total Energy Captured by the Battery	0.22491	kWh
Initial State of Charge (SOC0)	80	%

Final State of Charge (SOCF)	78.0157	%
Energy Difference from Initial Stored	0.10505	kWh
Distance Travelled	16.5061	km
Time of the Trip	766 (12.7667)	seconds (minutes)
Average Speed	77.5741	km/h
Cost of Operation	2.391	\$
Total H2 Consumption	161.392	grams
The hydrogen consumption	0.97777	kg / 100 km
The Current Tank Capacity Drives the Vehicle for	511.3652	km

Table 7.2 Simulation Results for Highway in CS Mode

7.2 FUDS

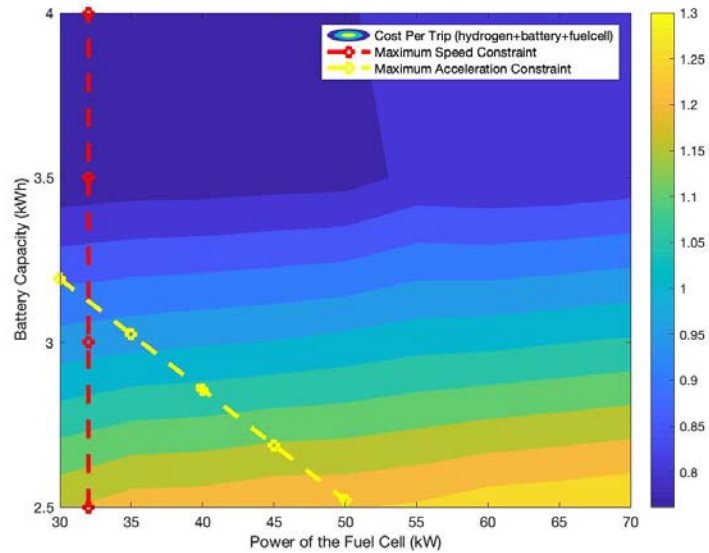


Figure 7.5 Trip Cost Contour Plot for FUDS Driving Cycle

Figure 7.5 shows the contour plot of the sizing optimization on the FUDS. The optimal and feasible size combination for battery capacity and fuel cell combination is 3.5 kWh and 35 kW respectively.

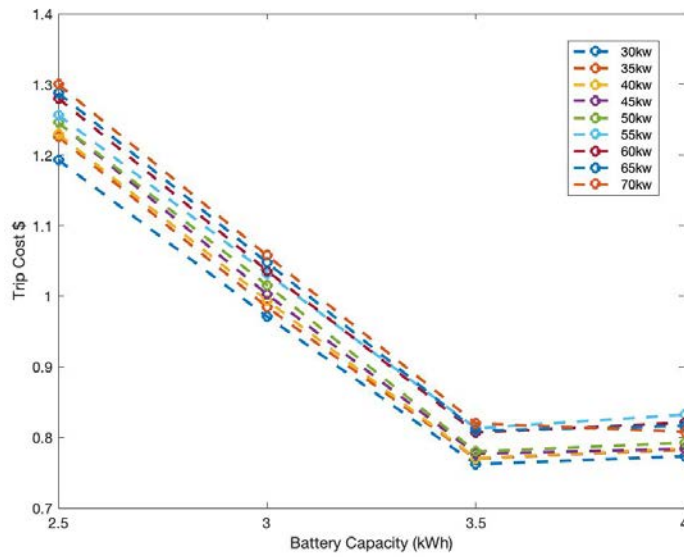
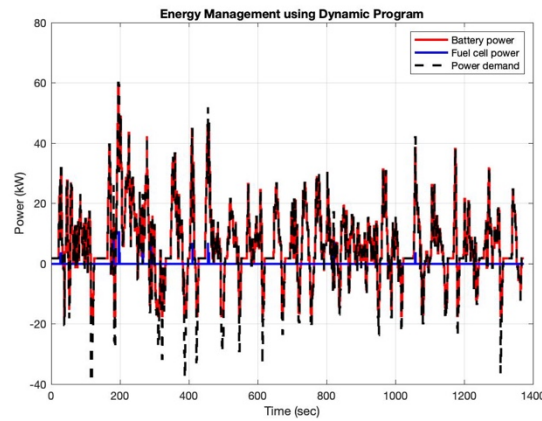


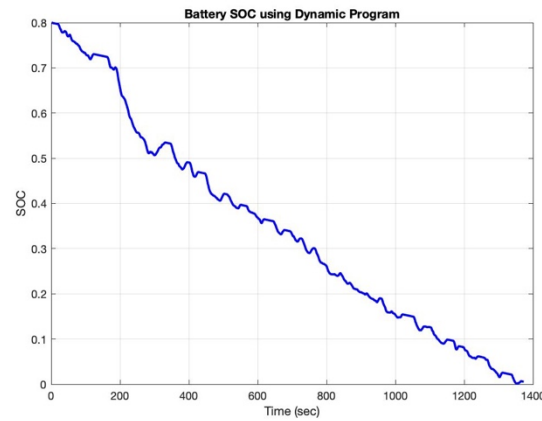
Figure 7.6 Pareto Front for FUDS Driving Cycle

Figure 7.6 shows the resulting Pareto front which represents the best trade-off between the two conflicting objectives which are reducing the trip cost and reducing the number of batteries for the different fuel cell sizes. As per the plot in figure 7.6, the best fuel cell size is 30 kw, but as per the contour plot in figure 7.5, this solution is not feasible.

7.2.1 CD Mode



(a)



(b)

Figure 7.7 Power Allocation and SOC for CD Mode – FUDS

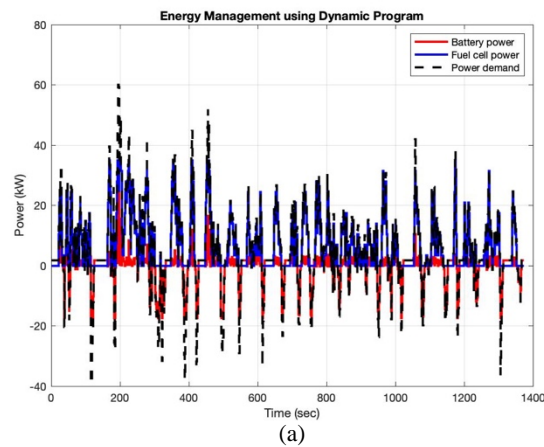
As shown in figure 7.7, the operation mode is CD, the power is mainly supplied by the battery and the battery keeps on depleting until the trip ends. The initial SOC was 80% and the final SOC was approximately 0.5%. The total energy supplied by the battery is greater than the energy supplied by the fuel cell. The energy captured by the battery from regenerative braking is 21% from the total energy required for the trip. Table 7.3 presents all the variables and results of the trip simulation.

The Power of the Fuel Cell	35	kW
The Size of the Battery	3.5	kWh
Initial Stored Energy in The Batteries	2.8	kWh
The total system weight	2150	kg
Total Energy Required for the trip	3.0475	kWh
Total Energy Supplied by the Fuel Cell	0.020417	kWh
Total Energy Supplied by the Battery	3.027	kWh

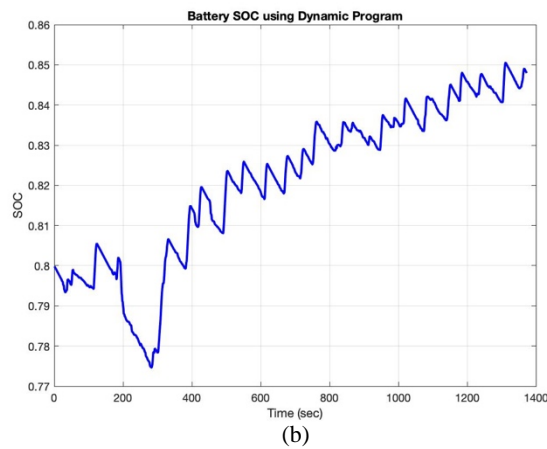
Total Energy Captured by the Battery	0.66333	kWh
Initial State of Charge (SOC0)	80	%
Final State of Charge (SOCF)	0.5474	%
Energy Difference from Initial Stored	3.2716	kWh
Distance Travelled	11.9896	km
Time of the Trip	1373 (22.8833)	seconds (minutes)
Average Speed	31.4368	km/h
Cost of Operation	0.75473	\$
Total H2 Consumption	1.176	grams
The hydrogen consumption	0.0098085	kg / 100 km
The Current Tank Capacity Drives the Vehicle for	50976.19412	km

Table 7.3 Simulation Results for FUDS in CD Mode

7.2.2 CS Mode



(a)



(b)

Figure 7.8 Power Allocation and SOC for CS Mode – FUDS

As shown in figure 7.8, the operation mode is CS, the power is mainly supplied by the fuel cell. The initial SOC was 80% and the final SOC was approximately 78%. Table 7.4 presents all the variables and results of the trip simulation.

The Power of the Fuel Cell	35	kW
The Size of the Battery	3.5	kWh
Initial Stored Energy in The Batteries	2.8	kWh
The total system weight	2150	kg
Total Energy Required for the trip	3.0475	kWh
Total Energy Supplied by the Fuel Cell	2.5268	kWh
Total Energy Supplied by the Battery	0.52378	kWh
Total Energy Captured by the Battery	0.66645	kWh
Initial State of Charge (SOC0)	80	%
Final State of Charge (SOCF)	84.7958	%
Energy Difference from Initial Stored	0.19747	kWh
Distance Travelled	11.9896	km
Time of the Trip	1373 (22.8833)	seconds (minutes)
Average Speed	31.4368	km/h
Cost of Operation	2.2995	\$
Total H2 Consumption	145.544	grams
The hydrogen consumption	1.2139	kg / 100 km
The Current Tank Capacity Drives the Vehicle for	411.8904	km

Table 7.4 Simulation Results for FUDS in CS Mode

7.3 NEDC

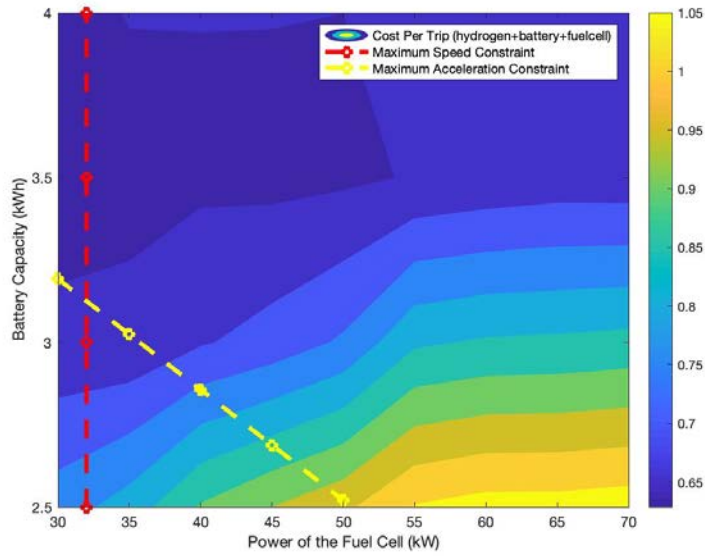


Figure 7.9 Trip Cost Contour Plot for NEDC Driving Cycle

Figure 7.9 shows the contour plot of the sizing optimization on the NEDC. The optimal and feasible size combination for battery capacities and fuel cell power size is 3.5 kWh and 45 kW respectively.

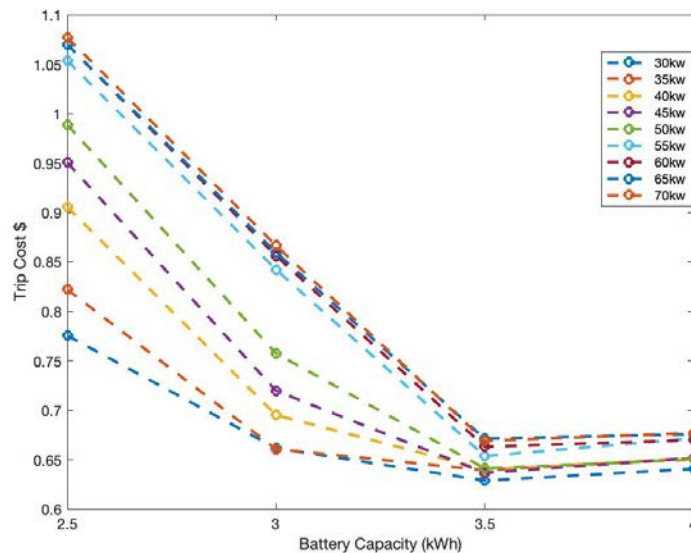


Figure 7.10 Pareto Front for NEDC Driving Cycle

Figure 7.10 shows the resulting Pareto front which represents the best trade-off between the two conflicting objectives which are reducing the trip cost and reducing the number of batteries for the different fuel cell sizes. As per the plot in figure 7.10,

the best fuel cell size is 30 kw, but as per the contour plot in figure 7.9, this solution is not feasible.

7.3.1 CD Mode

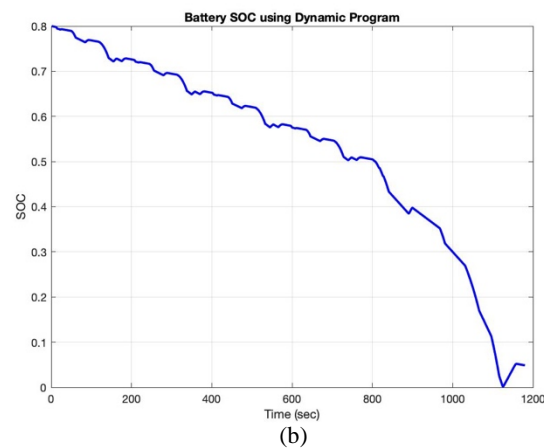
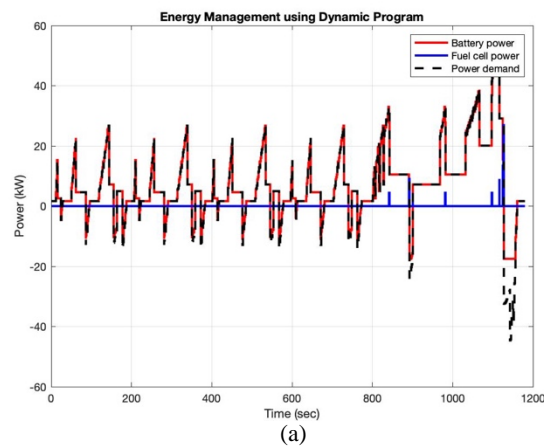


Figure 7.11 Power Allocation and SOC for CD Mode – NEDC

As shown in figure 7.11, the operation mode is CD, the power is mainly supplied by the battery and the battery keeps on depleting until the trip ends. The initial SOC was 80% and the final SOC was approximately 4.8%. The total energy supplied by the battery is much more than the energy supplied by the fuel cell. The energy captured by the battery from regenerative braking is 15% from the total energy required for the trip. Table 7.5 presents all the variables and results of the trip simulation.

The Power of the Fuel Cell	45	kW
The Size of the Battery	3.5	kWh
Initial Stored Energy in The Batteries	2.8	kWh
The total system weight	2173	kg
Total Energy Required for the trip	2.6657	kWh
Total Energy Supplied by the Fuel Cell	0.025	kWh
Total Energy Supplied by the Battery	2.6445	kWh
Total Energy Captured by the Battery	0.40915	kWh
Initial State of Charge (SOC0)	80	%
Final State of Charge (SOCF)	4.8625	%
Energy Difference from Initial Stored	3.0939	kWh
Distance Travelled	10.9314	km
Time of the Trip	1180 (19.6667)	seconds (minutes)
Average Speed	33.35	km/h
Cost of Operation	0.63112	\$
Total H2 Consumption	1.44	grams
The hydrogen consumption	0.013173	kg / 100 km
The Current Tank Capacity Drives the Vehicle for	37956.2114	km

Table 7.5 Simulation Results for NEDC in CD Mode

7.3.2 CS Mode

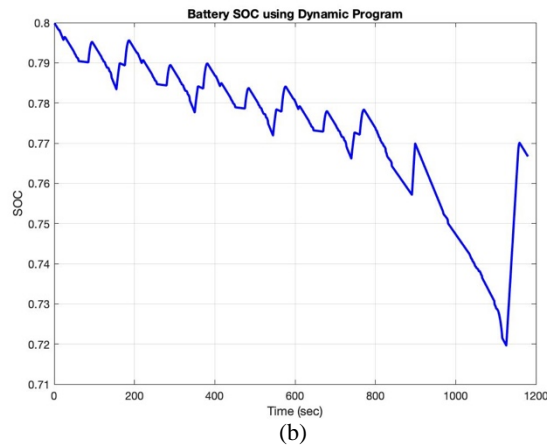
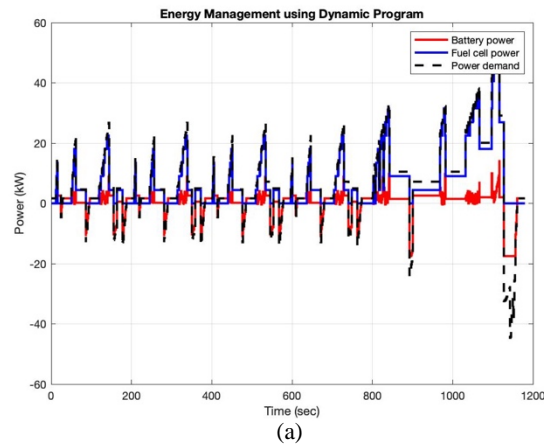


Figure 7.12 Power Allocation and SOC for CS Mode – NEDC

As shown in figure 7.12, the operation mode is CS, the power is mainly supplied by the fuel cell. The initial SOC was 80% and the final SOC was approximately 76%. Table 7.6 presents all the variables and results of the trip simulation.

The Power of the Fuel Cell	45	kW
The Size of the Battery	3.5	kWh
Initial Stored Energy in The Batteries	2.8	kWh
The total system weight	2173	kg
Total Energy Required for the trip	2.6657	kWh
Total Energy Supplied by the Fuel Cell	2.1612	kWh
Total Energy Supplied by the Battery	0.51006	kWh
Total Energy Captured by the Battery	0.41097	kWh
Initial State of Charge (SOC0)	80	%
Final State of Charge (SOCF)	76.6693	%

Energy Difference from Initial Stored	0.13715	kWh
Distance Travelled	10.9314	km
Time of the Trip	1180 (19.6667)	seconds (minutes)
Average Speed	33.35	km/h
Cost of Operation	1.9474	\$
Total H2 Consumption	124.488	grams
The hydrogen consumption	1.1388	kg / 100 km
The Current Tank Capacity Drives the Vehicle for	439.0539	km

Table 7.6 Simulation Results for NEDC in CS Mode

7.4 Summary

Characteristics	Unit	HIGHWAY	FUDS	NEDC
Distance	km	16.5	12	10.9
Time	sec	766	1373	1180
Max Speed	km/h	96.4	91.3	120
Average Speed	km/h	77.6	31.4	33.4
Max Acceleration	m/s ²	5	6.4	3.8
Max Deceleration	m/s ²	-5.3	-5.5	-5
From Pareto Front Results				
Best Fuel Cell Size	kW	35	35	45
Best Battery Size	kWh	4.5	3.5	3.5
CD Mode				
Battery Cost Weight	W _b	1	1	1
SOC0	%	80%	80%	80%
SOCF	%	4.97%	0.54%	4.86%
Total H2 Consumption	grams	0.45	1.18	1.44
Trip Cost	\$	0.67	0.75	0.63

CS Mode				
Battery Cost Weight	W _b	5	5	5
SOC ₀	%	80%	80%	80%
SOC _F	%	78.01%	84.79%	76.66%
Total H ₂ Consumption	grams	161.39	145.54	124.48
Trip Cost	\$	2.39	2.29	1.94
Cruising Range (5kg H ₂)	km	511	411	439
% of Regenerative Braking Energy	%	7	21	15

Table 7.7 Results Summary

Table 7.7 summarizes the results for all simulations and shows the best combination of power sources for each driving cycle. The summary table also shows that the fuel tank capacity, 5kg, is enough to run the vehicle more than 400 km on any of the three driving cycles. The importance of regenerative braking is depicted in this table also. The amount of regenerative braking ranges between 7 and 21 % of the total energy needed for the trip. The regenerative braking energy increases as the number of stop/start patterns increase during the trip. Moreover, it can be seen that the cost of the trip is always more expensive in CS mode because more hydrogen is consumed. However, the cost of recharging the battery back to its initial SOC is not considered in this thesis. For the CD mode, the resulting final SOC was approximately 0%, while, for the CS mode, the resulting final SOC falls within a range of +/- 5% of the initial SOC.

CHAPTER 8

CONCLUSION

This thesis presented an optimization approach to finding the optimal size combination for FCHV power sources to attain the least operational cost. TDP is an improved version of DP that removes the problem of dimensionality. This technique was used to determine the best power split to optimize the operational cost for a determined size combination. Battery selection is done based on several parameters to determine the most suitable type for this research which is Lithium Titanate. These types of batteries are characterized by its high-power capacity, high safety rating, high-performance rating, and low long-term cost. Two operational modes – CS and CD – are studied. CS mode is obtained by adding a weight cost factor of 5 to the optimization function. In CS mode, the final SOC lies within a 10% difference range of the initial SOC. Three drivability constraints were taken into consideration: maximum speed, maximum acceleration, and gradeability. These constraints helped to determine the possible sizes region and the minimum size of the electric motor (>123 kW). The Pareto front analysis was carried out to determine the optimum size of the fuel cell and battery for each driving cycle. The best size combinations obtained are 35 kW fuel cell and 4.5 kWh battery for the highway driving cycle; 35 kW fuel cell and 3.5 kWh battery for the FUDS; 45 kW fuel cell and 35 kWh battery for the NEDC. The size of the hydrogen tank chosen (5 kg) was enough to drive the car more than 400 km for all the driving cycles. Finally, the importance of the regenerative braking was also shown in the results; the amount of regenerative braking energy ranges from 7 to 21% depending on the driving cycle. This is considered to be a significant amount that should be made use of.

1: ABBREVIATIONS

CD: Charge depletion mode
CS: Charge sustaining mode
DP: Dynamic Programming
EMS: Energy system
FCHV: Fuel cell hybrid vehicles
FUDS: Federal Urban Driving Schedule
HEV: Hybrid electric vehicle
NEDC: National European Driving Cycle
SOC: Battery state of charge
TDP: Tunnel dynamic programming

REFERENCES

- Ahmadi, P., Torabi, S. H., Afsaneh, H., Sadegheih, Y., Ganjehsarabi, H., & Ashjaee, M. (2019). The effects of driving patterns and PEM fuel cell degradation on the lifecycle assessment of hydrogen fuel cell vehicles. *International Journal of Hydrogen Energy*.
- Ahmadi, S., Bathaee, S., & Hosseinpour, A. H. (2018). Improving fuel economy and performance of a fuel-cell hybrid electric vehicle (fuel-cell, battery, and ultra-capacitor) using optimized energy management strategy. *Energy conversion and management*, 160, 74-84.
- Amamou, A., Ziadia, M., Kelouwani, S., Agbossou, K., & Dube, Y. (2018). *Fuel-Cell and Battery Hybrid Source Optimal Power Management for Electric Mobility*. Paper presented at the 2018 IEEE Vehicle Power and Propulsion Conference (VPPC).
- Aschilean, I., Varlam, M., Culcer, M., Iliescu, M., Raceanu, M., Enache, A., . . . Filote, C. (2018). Hybrid electric powertrain with fuel cells for a series vehicle. *Energies*, 11(5), 1294.
- Battery Univeristy. (2016, July 21). Bu-216: Summary table of lithium-based batteries. Retrieved from https://batteryuniversity.com/learn/article/bu_216_summary_table_of_lithium_based_batteries
- Battery Univeristy. (2018, May 31). Bu-205: Types of lithium-ion.
- Bizon, N., & Thounthong, P. (2018). Real-time strategies to optimize the fueling of the fuel cell hybrid power source: A review of issues, challenges and a new approach. *Renewable and Sustainable Energy Reviews*, 91, 1089-1102.
- Cano, Z. P., Banham, D., Ye, S., Hintennach, A., Lu, J., Fowler, M., & Chen, Z. (2018). Batteries and fuel cells for emerging electric vehicle markets. *Nature Energy*, 3(4), 279.
- da Fonseca, R., Bideaux, E., Jeanneret, B., Gerard, M., Desbois-Renaudin, M., & Sari, A. (2012). *Energy management strategy for hybrid fuel cell vehicle*. Paper presented at the 2012 12th International Conference on Control, Automation and Systems.
- Denis, N., Dubois, M. R., Trovão, J. P. F., & Desrochers, A. (2018). Power split strategy optimization of a plug-in parallel hybrid electric vehicle. *IEEE Transactions on Vehicular Technology*, 67(1), 315-326.
- Dinnawi, R., Fares, D., Chedid, R., Karaki, S., & Jabr, R. A. (2014). *Optimized energy management system for fuel cell hybrid vehicles*. Paper presented at the MELECON 2014-2014 17th IEEE Mediterranean Electrotechnical Conference.
- Fares, D., Chedid, R., Karaki, S., Jabr, R., Panik, F., Gabele, H., & Huang, Y. (2014). Optimal power allocation for a FCHV based on linear programming and PID controller. *International Journal of Hydrogen Energy*, 39(36), 21724-21738.
- Fares, D., Chedid, R., Panik, F., Karaki, S., & Jabr, R. (2015). Dynamic programming technique for optimizing fuel cell hybrid vehicles. *International Journal of Hydrogen Energy*, 40(24), 7777-7790.
- Fathabadi, H. (2018). Novel fuel cell/battery/supercapacitor hybrid power source for fuel cell hybrid electric vehicles. *Energy*, 143, 467-477.

- Fathabadi, H. (2019). Combining a proton exchange membrane fuel cell (PEMFC) stack with a Li-ion battery to supply the power needs of a hybrid electric vehicle. *Renewable Energy*, *130*, 714-724.
- Fletcher, T., Thring, R., & Watkinson, M. (2016). An energy management strategy to concurrently optimise fuel consumption & PEM fuel cell lifetime in a hybrid vehicle. *International Journal of Hydrogen Energy*, *41*(46), 21503-21515.
- Geng, C., Jin, X., & Zhang, X. (2019). Simulation research on a novel control strategy for fuel cell extended-range vehicles. *International Journal of Hydrogen Energy*, *44*(1), 408-420.
- Hu, X., Murgovski, N., Johannesson, L. M., & Egardt, B. (2015). Optimal dimensioning and power management of a fuel cell/battery hybrid bus via convex programming. *IEEE/ASME transactions on mechatronics*, *20*(1), 457-468.
- Karaki, S. H., Dinnawi, R., Jabr, R., Chedid, R., & Panik, F. (2015). Fuel cell hybrid electric vehicle sizing using ordinal optimization. *SAE International Journal of Passenger Cars-Electronic and Electrical Systems*, *8*(2015-01-0155), 60-69.
- Karaki, S. H., Jabr, R., Chedid, R., & Panik, F. (2015). *Optimal energy management of hybrid fuel cell electric vehicles* (0148-7191). Retrieved from
- Karaođlan, M. U., Kuralay, N. S., & Colpan, C. O. (2019). The effect of gear ratios on the exhaust emissions and fuel consumption of a parallel hybrid vehicle powertrain. *Journal of Cleaner Production*, *210*, 1033-1041.
- Koniak, M., & Czerepicki, A. (2017). *Selection of the battery pack parameters for an electric vehicle based on performance requirements*. Paper presented at the IOP Conference Series: Materials Science and Engineering.
- Li, Q., Huang, W., Chen, W., Yan, Y., Shang, W., & Li, M. (2019). Regenerative braking energy recovery strategy based on Pontryagin's minimum principle for fuel cell/supercapacitor hybrid locomotive. *International Journal of Hydrogen Energy*, *44*(11), 5454-5461.
- Lü, X., Qu, Y., Wang, Y., Qin, C., & Liu, G. (2018). A comprehensive review on hybrid power system for PEMFC-HEV: Issues and strategies. *Energy conversion and management*, *171*, 1273-1291.
- Marx, N., Hissel, D., Gustin, F., Boulon, L., & Agbossou, K. (2017). On the sizing and energy management of an hybrid multistack fuel cell–Battery system for automotive applications. *International Journal of Hydrogen Energy*, *42*(2), 1518-1526.
- Odeim, F., Roes, J., & Heinzl, A. (2015). Power management optimization of an experimental fuel cell/battery/supercapacitor hybrid system. *Energies*, *8*(7), 6302-6327.
- Odeim, F., Roes, J., & Heinzl, A. (2016). Power management optimization of a fuel cell/battery/supercapacitor hybrid system for transit bus applications. *IEEE Transactions on Vehicular Technology*, *65*(7), 5783-5788.
- Odeim, F., Roes, J., Wülbeck, L., & Heinzl, A. (2014). Power management optimization of fuel cell/battery hybrid vehicles with experimental validation. *Journal of Power Sources*, *252*, 333-343.
- Roda, V., Carroquino, J., Valiño, L., Lozano, A., & Barreras, F. (2018). Remodeling of a commercial plug-in battery electric vehicle to a hybrid configuration with a PEM fuel cell. *International Journal of Hydrogen Energy*, *43*(35), 16959-16970.

- Rurgladdapan, J., Uthaichana, K., & Kaewkham-ai, B. (2013). *Optimal Li-Ion battery sizing on PEMFC hybrid powertrain using dynamic programming*. Paper presented at the 2013 IEEE 8th Conference on Industrial Electronics and Applications (ICIEA).
- Sarma, U., & Ganguly, S. (2018). Determination of the component sizing for the PEM fuel cell-battery hybrid energy system for locomotive application using particle swarm optimization. *Journal of Energy Storage, 19*, 247-259.
- Song, Z., Zhang, X., Li, J., Hofmann, H., Ouyang, M., & Du, J. (2018). Component sizing optimization of plug-in hybrid electric vehicles with the hybrid energy storage system. *Energy, 144*, 393-403.
- Store, F. C. (2013). 5000W Fuel Cell Stack user Manual.
- Sulaiman, N., Hannan, M., Mohamed, A., Ker, P., Majlan, E., & Daud, W. W. (2018). Optimization of energy management system for fuel-cell hybrid electric vehicles: Issues and recommendations. *Applied Energy, 228*, 2061-2079.
- Taherzadeh, E., Dabbaghjamanesh, M., Gitizadeh, M., & Rahideh, A. (2018). A new efficient fuel optimization in blended charge depletion/charge sustenance control strategy for plug-in hybrid electric vehicles. *IEEE Transactions on Intelligent Vehicles, 3*(3), 374-383.
- Tazelaar, E., Shen, Y., Veenhuizen, P., Hofman, T., & Van den Bosch, P. (2012). Sizing stack and battery of a fuel cell hybrid distribution truck. *Oil & Gas Science and Technology—Revue d'IFP Energies nouvelles, 67*(4), 563-573.
- Tazelaar, E., Veenhuizen, B., & Grimminck, M. (2012). Analytical solution of the energy management for fuel cell hybrid propulsion systems. *IEEE Transactions on Vehicular Technology, 61*(5), 1986-1998.
- Vinot, E., Reinbold, V., & Trigui, R. (2016). Global optimized design of an electric variable transmission for HEVs. *IEEE Transactions on Vehicular Technology, 65*(8), 6794-6798.
- Wang, X., He, H., Sun, F., & Zhang, J. (2015). Application study on the dynamic programming algorithm for energy management of plug-in hybrid electric vehicles. *Energies, 8*(4), 3225-3244.
- Xiao, R., Liu, B., Shen, J., Guo, N., Yan, W., & Chen, Z. (2018). Comparisons of energy management methods for a parallel plug-in hybrid electric vehicle between the convex optimization and dynamic programming. *Applied Sciences, 8*(2), 218.
- Zheng, C., Xu, G., Jeong, J., Cha, S. W., Park, Y.-i., & Lim, W. (2014). Power source sizing of fuel cell hybrid vehicles considering vehicle performance and cost. *International journal of precision engineering and manufacturing, 15*(3), 527-533.